Reconstructing ATLAS SU3 in the CMSSM and relaxed phenomenological supersymmetry models

Andrew Fowlie*
Department of Physics and Astronomy, University of Sheffield, Sheffield S3 7RH, England

Leszek Roszkowski†
The Andrzej Soltan Institute for Nuclear Studies, Hoza 69, 00-681 Warsaw, Poland, and
Department of Physics and Astronomy, University of Sheffield, Sheffield S3 7RH, England

(Dated: June 28, 2011)

Assuming that the LHC makes a positive end-point measurement indicative of low-energy supersymmetry, we examine the prospects of reconstructing the parameter values of a typical low-mass point in the framework of the Constrained MSSM and in several other supersymmetry models that have more free parameters and fewer assumptions than the CMSSM. As a case study, we consider the ATLAS SU3 benchmark point with a Bayesian approach and with a Gaussian approximation to the likelihood for the measured masses and mass differences. First we investigate the impact of the hypothetical ATLAS measurement alone and show that it significantly narrows the confidence intervals of relevant, otherwise fairly unrestricted, model parameters. Next we add information about the relic density of neutralino dark matter to the likelihood and show that this further narrows the confidence intervals. We confirm that the CMSSM has the best prospects for parameter reconstruction; its results had little dependence on our choice of prior, in contrast to the other models that we study where the situation is less clear. By comparing parameter reconstruction we find that sometimes gaugino mass unification, rather than having fewer free parameters, is critical. We also study prospects for evaluating the relic density of neutralino dark matter from LHC data alone and for direct detection searches with information from both LHC data and the relic density of dark matter. Finally we perform a brief comparison of parameter and relevant mass reconstruction in the models that we study.

I. INTRODUCTION

The search for supersymmetry (SUSY) at the LHC is now in full swing [1–3]. Assuming that the LHC makes a specific positive measurement, we investigate whether the measurement could be explained by various SUSY models, and whether the measurement could be used to distinguish among them and to determine their parameters [4, 5]. As a case study, we consider the ATLAS SU3 benchmark point [6], a typical low-mass scenario. If a mass spectrum similar to the one of the SU3 point were realised in nature, LHC measurements of dilepton edges would allow one to determine one mass and three mass differences with correlated uncertainties. Taking this as input, within a Bayesian statistical approach we will attempt to reconstruct the ATLAS SU3 benchmark point in five supersymmetry models. For each model, we will find the regions of the model's parameter space that are in best agreement with the one mass and three mass differences that the LHC would measure. Next, we will examine the extent to which providing additional information from the relic density of the lightest neutralino as the lightest supersymmetric particle (LSP) will help further improve the determination of the parameters. We will find these regions with an adapted version of the publicly available `SuperBayeS` computer program [7–10]. Then, we will see whether we have reconstructed the ATLAS SU3 benchmark point, that is, whether the regions that we have found closely envelop the ATLAS SU3 benchmark point.

We consider five phenomenological models of supersymmetry. The Constrained Minimal Supersymmetric Standard Model (Constrained MSSM, or CMSSM) [11] is the most economical model; it has only four free continuous parameters: the common gaugino mass $m_{1/2}$, the common scalar mass m_0, the common trilinear term A_0, all defined at the GUT scale, plus the ratio of the Higgs vacuum expectation values $\tan\beta$, defined at the electroweak (EW) scale. Because of its simplicity, the CMSSM is a tractable model that is well studied, and despite its restrictive boundary conditions, the CMSSM allows a wide range of phenomenology.

There are, however, theoretical reasons for considering "relaxed" models; models in which some parameters are free at the GUT scale. The Non-Universal Higgs Model (NUHM) can be viewed as a relaxed version of the CMSSM. In

*Electronic address: A.Fowlie@sheffield.ac.uk
†Electronic address: L.Roszkowski@sheffield.ac.uk

the NUHM, the Higgs soft masses are free parameters at the GUT scale, unlike in the CMSSM, where they unify with the common scalar mass. Assuming Higgs mass unification with other scalar masses at the GUT scale is not well motivated, because the Higgs and the scalar fermions belong to different supermultiplets. The NUHM has two more parameters than the CMSSM, namely the Higgs soft masses m_{H_u} and m_{H_d}, and it has a richer phenomenology involving Higgs bosons [12–14].

Another relaxed phenomenological alternative to the CMSSM that we will consider is the CMSSM with non-universal gaugino masses (CMSSM-NUG). In contrast to the CMSSM's gaugino soft masses, the CMSSM-NUG's gaugino soft masses will not unify at the GUT scale; they are free parameters. The CMSSM-NUG has more freedom than the CMSSM, for instance, unlike in the CMSSM, in the CMSSM-NUG, LEP bounds for neutralino masses cannot be derived from LEP bounds for chargino masses. The CMSSM-NUG has two additional parameters; the common gaugino mass is replaced by three independent gaugino soft mass parameters for the bino (M_1), the wino (M_2) and the gluino (M_3).

Furthermore, we consider the MSSM, with all the parameters defined at the EW scale. The general MSSM has over one hundred free parameters. We, however, reduce the MSSM's number of free parameters, first by imposing the condition of minimal flavour violation in order to satisfy strong bounds on CP-violation and flavour changing neutral currents, and second by assuming some unification at the GUT scale and some degeneracy at the EW scale, so that the resulting model is tractable. Our MSSM has twelve free parameters, which are defined at the EW scale, and are listed below.

Finally, we relax our MSSM by lifting the assumption of gaugino mass unification. We study the MSSM where the gaugino soft masses are free parameters that are defined at the EW scale, and call the model the Non-Universal Gaugino MSSM or MSSM-NUG. In contrast to the MSSM mentioned above, the MSSM-NUG has fourteen free parameters, which are defined at the EW scale, and are listed below.

Our work is an extension of Ref. [15] where the SU3 parameter reconstruction was performed within the framework of the CMSSM only and in which more optimistic uncertainties in computing the neutralino's relic density were assumed. Otherwise we will follow a similar methodology and apply it to the models listed above. Additionally, here we will make an important preliminary step, which will be to delineate the most likely regions of the parameter space (for every model) by imposing physicality constraints alone, before applying information from an assumed ATLAS measurement or dark matter density. Our main aim in this paper will be to assess the feasibility of reconstructing the SU3 point in the CMSSM and the other SUSY models that we consider here.

The paper is organised as follows. In section II, we discuss the ATLAS SU3 benchmark point and the positive measurements that would be possible at the LHC were Nature described by ATLAS SU3. In section III, we detail our methodology, showing how we construct our likelihood function and describing our Bayesian statistical approach. In section IV, we present the results of our scans of the CMSSM, NUHM, CMSSM-NUG, MSSM, and MSSM-NUG for the reconstruction of the model parameters. We also compare each model's Bayesian evidence, and present properties of each model relevant to dark matter density and searches. Lastly, we summarise our study in section V.

II. THE ATLAS SU3 BENCHMARK POINT

In preparation for conducting SUSY searches, LHC Collaborations adopted a set of "benchmark points" in the CMSSM and some other models. At each benchmark point, the CMSSM has a distinct phenomenological set of signals. In particular, the ATLAS Collaboration defined the SU3 benchmark point [6] which is specified in Table I. We calculated the CMSSM's sparticle mass spectrum at ATLAS SU3 with `SOFTSUSY` [16]. It is shown in Table II and Figure 1.

CMSSM parameter	ATLAS SU3 point	SM parameter	Input value
$m_{1/2}$	300 GeV	M_t	172.6 GeV
m_0	100 GeV	$m_b(m_b)^{\overline{MS}}$	4.20 GeV
$\tan\beta$	6.0	$\alpha_s(M_Z)^{\overline{MS}}$	0.1176
A_0	-300 GeV	$1/\alpha_{\rm em}(M_Z)^{\overline{MS}}$	127.955
$\mathrm{sgn}\,\mu$	$+$		

TABLE I: Left side: input CMSSM parameter values for the ATLAS SU3 benchmark point. Right side: input values of relevant SM parameters used in our numerical analysis.

Whilst the SU3 point was originally defined in the CMSSM, we extend its definition to the other models considered here as follows. In the NUHM and the CMSSM-NUG, ATLAS SU3 is defined as it was in the CMSSM in Table I, but with $m_{H_d} = m_{H_u} = m_0$ and $M_1 = M_2 = M_3 = m_{1/2}$, respectively. In the MSSM and MSSM-NUG, ATLAS SU3

Sparticle	Mass (GeV)				
$\chi_1^0 = \chi$	117.9	$\tilde{e}_L$, $\tilde{\mu}_L$	230.8	$\tilde{d}_L$	666.2
χ_2^0	223.4	$\tilde{e}_R$, $\tilde{\mu}_R$	157.5	$\tilde{d}_R$	639.0
χ_3^0	463.8	$\tilde{\nu}_e$, $\tilde{\nu}_\mu$	217.5	$\tilde{u}_L$	660.3
χ_4^0	479.9	$\tilde{\tau}_1$	152.2	$\tilde{u}_R$	644.3
$\chi_1^\pm$	224.4	$\tilde{\tau}_2$	232.4	$\tilde{b}_1$	599.0
$\chi_2^\pm$	476.4	$\tilde{\nu}_\tau$	216.9	$\tilde{b}_2$	636.6
$\tilde{g}$	717.5			$\tilde{t}_1$	446.9
				$\tilde{t}_2$	670.9

TABLE II: The sparticle mass spectrum in the CMSSM at the ATLAS SU3 benchmark point, calculated with `SOFTSUSY`.

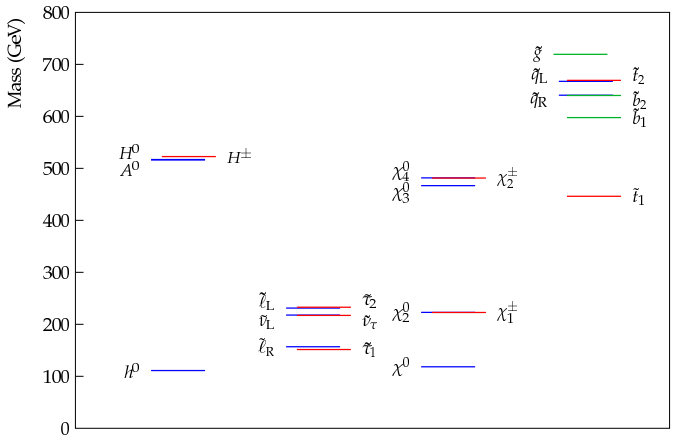

FIG. 1: The mass spectrum for the ATLAS SU3 benchmark point.

is found by running the CMSSM parameters to the EW scale with `SOFTSUSY` to obtain ATLAS SU3 for a general MSSM, and then averaging the parameters that are degenerate in our MSSM. The resulting parameters for ATLAS SU3 in the MSSM are shown in Table III. Because the MSSM parameters at the SUSY mass scale will be the same in all the models, the physical sparticle mass spectrum corresponding to the ATLAS SU3 point will also be the same in all the models.

Parameter	Description	ATLAS SU3 value (masses in GeV)
MSSM:		
M_2	Wino mass	231
m_L	Left-handed slepton mass	224
m_E	Right-handed slepton mass	149
m_Q	Left-handed squark mass	622
m_U	Right-handed up-type-squark mass	574
m_D	Right-handed down-type-squark mass	618
A_U	Up-type-quark trilinear coupling	-824
A_D	Down-type-quark trilinear coupling	-1164
A_L	Lepton trilinear coupling	-486
m_A	Pseudoscalar Higgs mass	462
μ	Higgs parameter	521
$\tan\beta$	Ratio of Higgs vevs	6
MSSM-NUG: MSSM parameters plus:		
M_1	Bino mass	123
M_3	Gluino mass	696

TABLE III: Input MSSM and MSSM-NUG parameter values for the ATLAS SU3 benchmark point.

One promising way of discovering supersymmetry at the LHC is to study a squark decay chain [6]. A squark can

decay, via intermediate states, to the lightest neutralino, a pair of leptons and a quark,

$$\tilde{q}_L \to \chi_2^0 q \to \tilde{l}^{\pm} l^{\mp} q \to \chi l^+ l^- q, \tag{1}$$

where $\widetilde{q}_L$ denotes the first or second generation left squark, $\chi_1^0 = \chi$ and χ_2^0 the first and second neutralino and $\widetilde{l}$ an intermediate slepton.

The experimental signature for this chain will be two leptons with opposite signs, a hard jet and missing energy. By measuring the invariant masses of outgoing particles,

$$M^2 = \left(\sum E\right)^2 - \left|\sum \vec{P}\right|^2, \tag{2}$$

one can determine relationships between the masses of the particles in the decay chain in Eq. 1.

For the ATLAS SU3 benchmark point, the decay chain in Eq. 1 will swamp other processes, because sleptons are lighter than χ_2^0. The invariant mass distribution for the lepton pair will be triangular, like a single sawtooth. The position of the edge of the invariant mass distribution is dependent on the sparticle mass hierarchy; for ATLAS SU3 it will be

$$M_{ll,\,\mathrm{edge}}^2 = m_{\chi_2^0}^2 \left[1 - \left(\frac{m_{\tilde{l}}}{m_{\chi_2^0}}\right)^2\right] \left[1 - \left(\frac{m_\chi}{m_{\tilde{l}}}\right)^2\right]. \tag{3}$$

Measuring $M_{ll,\,\mathrm{edge}}$ gives a relationship between $m_{\chi_2^0}$, $m_{\tilde{l}}$ and m_χ. Measuring other invariant mass edges allows one to determine all the masses involved in the decay chain in Eq. 1. The squark flavours, however, will be indistinguishable, and the lightest slepton will dominate the decay chain. The set of measurable masses is, therefore,

$$\theta = \left(m_\chi, m_{\chi_2^0} - m_\chi, m_{\tilde{q}} - m_\chi, m_{\tilde{l}} - m_\chi\right), \tag{4}$$

where

$$m_{\tilde{q}} = \frac{1}{4}\left(m_{\tilde{u}_R} + m_{\tilde{u}_L} + m_{\tilde{d}_R} + m_{\tilde{d}_L}\right), \tag{5}$$

$$m_{\tilde{l}} = \min\left(m_{\tilde{e}_R}, m_{\tilde{e}_L}, m_{\tilde{\mu}_R}, m_{\tilde{\mu}_L}, m_{\tilde{\tau}_1}, m_{\tilde{\tau}_2}\right). \tag{6}$$

The mass measurements will be correlated; the covariance matrix (which is is the inverse of the Fisher matrix) that describes their correlation for the ATLAS SU3 benchmark point is shown in Table IV.[1] It was obtained by ATLAS assuming an integrated luminosity of $1\,\mathrm{fb}^{-1}$ and a positive measurement of the decay chain given by Eq. 1 or the high-p_T and large missing energy decay chain $\widetilde{q}_R \to \chi q$, where $\widetilde{q}_R$ denotes the first or second generation right squark.

	m_χ	$m_{\chi_2^0} - m_\chi$	$m_{\tilde{q}} - m_\chi$	$m_{\tilde{l}} - m_\chi$
m_χ	3.72×10^3	53.4	1.92×10^3	1.075×10^2
$m_{\chi_2^0} - m_\chi$		3.6	29.0	-1.3
$m_{\tilde{q}} - m_\chi$			1.12×10^3	4.65
$m_{\tilde{l}} - m_\chi$				14.1

TABLE IV: The ATLAS SU3 covariance matrix. All entries have dimension GeV^2.

The central values for the mass measurements for the ATLAS SU3 benchmark point are shown in Table V. They were calculated with `SOFTSUSY`. Table V also shows the simulated relic density for ATLAS SU3, with an error from WMAP5 [17]. The ATLAS SU3 benchmark point is in the "bulk region" of the CMSSM's parameter space. In this region, neutralino co-annihilation is dominated by slepton exchange, and the neutralino's relic density is typically of the correct order of magnitude, without excessive fine-tuning.

We calculated the neutralino's relic density in the CMSSM at ATLAS SU3 with `micrOMEGAs` [18, 19]. The calculated relic density, ${\Omega_\chi h^2}_{\mathrm{SU3}} = 0.2332$, exceeds, and is in statistically significant disagreement with, WMAP5's measurement, $\Omega h^2{}_{\mathrm{WMAP}} = 0.1099 \pm 0.0062$ [17]. The ATLAS SU3 benchmark point is, however, representative of similar points that result in neutralino's with relic densities that are in agreement with WMAP's measurement. By increasing the value of $\tan\beta$, one can increase the neutralino's higgsino component. The neutralino's higgsino component enhances $\chi\chi \to WW$ annihilation, and, consequently, suppresses the neutralino's relic density. Clearly, then, one can adjust the value of $\tan\beta$ so that the neutralino's relic density is in agreement with WMAP's measurement.

[1] We have corrected some typos in the covariance matrix given in Ref. [15].

Quantity	Mean (masses in GeV)	Error
Simulated LHC measurement		
m_χ	117.9	See covariance matrix
$m_{\chi_2^0} - m_\chi$	105.5	See covariance matrix
$m_{\tilde{q}} - m_\chi$	534.5	See covariance matrix
$m_{\tilde{l}} - m_\chi$	34.3	See covariance matrix
Simulated WMAP measurement		
$\Omega_\chi h^2$	0.2332	6.2×10^{-3}

TABLE V: The five ATLAS SU3 measurable quantities used in this analysis.

III. METHOD

In evaluating prospects for reconstructing the SU3 point in different SUSY models we will proceed in three steps. Firstly, we will delineate the regions of parameters which are physically allowed, as described below. Next, we will add information that the supposed ATLAS edge measurement would provide. Finally, we will examine the impact of additionally assuming that the neutralino's relic density at the SU3 point is correct.

We perform our numerical analysis with the help of `SuperBayeS` [7–10] — a sophisticated computer program that fits a model's free parameters to experimental data using Bayesian statistical techniques. It uses Monte Carlo methods to find the regions of parameter space that are in best agreement with experimental data (the regions where the posterior is maximised). `SuperBayeS` includes the programs `SOFTSUSY`, which computes mass spectra, `micrOMEGAs`, which computes the neutralino's relic density and direct detection cross section, and `MultiNest` [20], a scanning routine that employs nested sampling (NS).

The pertinent statistical quantities are calculated numerically, after the list of points has been "binned." The points are binned by dividing the parameter space into "bins" and counting the number of points in each bin. The posterior is proportional to the number of points in each bin. The profile likelihood[2] is found by finding the bin with the highest likelihood, within the set of bins where the parameter of interest is constant. The marginalised posterior is found by summing the bin widths multiplied by the posterior for that bin, within the set of bins where the parameter of interest is constant. The best-fit point is found by finding the bin with the greatest likelihood. The posterior mean is found by summing all the bin widths multiplied by the parameter of interest and the posterior. The evidence is found by summing the likelihood of each closed contour multiplied by the prior volume in each closed contour. The marginalised posteriors and profile likelihoods are normalised by setting their maximum values to unity.

We adapted the `SuperBayeS` computer program so that it scanned over the five phenomenological supersymmetry models discussed in section I,[3] so that it included a simulated value for the neutralino's relic density, and so that it included simulated LHC constraints in its likelihood function. The likelihood in our adapted codes is the product of contributions from the LHC edge measurements and the WMAP dark matter density; $\mathcal{L} = \mathcal{L}_{\rm LHC} \times \mathcal{L}_{\rm DM}$, where

$$-2\ln\mathcal{L}_{\rm LHC} = (\theta - \theta_{\rm SU3})\, C^{-1}\, (\theta - \theta_{\rm SU3})^T\,, \tag{7}$$

$$-2\ln\mathcal{L}_{\rm DM} = \frac{\left(\Omega_\chi h^2 - {\Omega_\chi h^2}_{\rm SU3}\right)^2}{\sigma^2_{\rm CALC} + \sigma^2_{\rm WMAP}}, \tag{8}$$

where θ is the parameter set in Eq. 4, $\theta_{\rm SU3}$ is given in Table V and C is the covariance matrix in Table IV, $\Omega_\chi h^2$ is the neutralino's relic density calculated at a scanned point, ${\Omega_\chi h^2}_{\rm SU3}$ is the neutralino's relic density at the ATLAS SU3 point, given in Table V, $\sigma^2_{\rm WMAP}$ is the WMAP5 error, given in Table V, $\sigma^2_{\rm CALC}$ is the theoretical error in the neutralino's relic density. Evidently, we have assumed that the likelihood functions are Gaussians, that is, that the measured values (the ATLAS SU3 values) are described by Gaussians centred on the calculated values.

The theoretical error for the neutralino's relic density in Eq. 8, $\sigma_{\rm CALC}$, results from errors in the sparticle mass spectrum, rather than from numerical errors or approximations within the relic density calculation itself. These errors originate from approximations that are made when adding radiative corrections to the sparticle masses.[4] It

[2] In evaluating the profile likelihood for a given parameter (or set of parameters) one maximises the likelihood along the other parameters of the model, in contrast to the marginalised posterior, where one integrates over them; see Ref. [15] for more details.

[3] The MSSM-NUG code was written by Roberto Ruiz de Austri.

[4] These errors in the sparticle mass spectrum are negligible in Eq. 7, because they are much smaller than the entries in the covariance matrix.

was asserted in a previous study, Ref. [15], that $\sigma_{\rm CALC}$ will be negligible in the CMSSM's bulk region. We, however, haven't studied the theoretical error in the NUHM, CMSSM-NUG, MSSM or MSSM-NUG. Whilst the theoretical error at ATLAS SU3 will be the same in all the models (because the MSSM parameters at the SUSY mass scale will be the same), we don't know how the theoretical error will behave around ATLAS SU3 in each model. Furthermore, we used an on-line comparison tool[5] to estimate $\sigma_{\rm CALC}$ at the ATLAS SU3 benchmark point. The comparison tool calculated the sparticle mass spectrum at ATLAS SU3 with three different RGE codes, then calculated the relic density resulting from each sparticle mass spectrum with `micrOMEGAs`. The differences between the relic densities were of order 5-10%. We, therefore, cautiously take $\sigma_{\rm CALC} = 0.1\Omega_\chi h^2{}_{\rm CALC}$ (that is, 10%), which is its default value for the CMSSM in `SuperBayeS`.

`SuperBayeS` rejects points in a model's parameter space that are unphysical; they are assigned zero prior probability. The potential physicality problems are listed in Table VI. Because unphysical points are rejected in this way, a model's priors are correlated in a complicated way. The resulting marginalised priors will not be sharp, step-function distributions — priors that evenly weight orders of magnitude (log priors) will have a $1/x$ shape and regions of parameter space with more physical points will have a greater prior probability.

Physicality problems
No radiative electroweak symmetry breaking; b has the wrong sign
No radiative electroweak symmetry breaking; μ^2 has the wrong sign
Tachyonic Higgs
Tachyonic sfermion
Landau pole in renormalisation group evolution
No electroweak symmetry breaking; μ cannot be calculated
No electroweak symmetry breaking minimum
Landau pole; infra-red quasi-fixed point breached
Desired accuracy cannot be reached
Lightest neutralino is not the LSP

TABLE VI: The potential physicality problems. If a point has one or more of these problems, it is unphysical.

We ran our modified `SuperBayeS` programs with the NS algorithm on a high-performance computer three times. First, we ran them with no constraints other than the physicality conditions. Second, we did the same but this time applied simulated LHC constraints. Third, we ran them with simulated LHC and simulated WMAP constraints. For mass parameters, we used prior ranges that equally weighted orders of magnitude (log priors). The priors that we used are listed in Table VII. Because of their experimental uncertainties, the nuisance parameters are varied around their mean experimental values. We, however, did not include a likelihood from measurements of the nuisance parameters in our likelihood function.

Our chosen NS parameters were such that the NS algorithm would accurately map the posterior (but not the profile likelihood) and accurately calculate the evidence, in a reasonable CPU time. Accurately mapping the profile likelihood with NS requires more CPU time. The technical details of our runs are listed in Table VIII.

IV. RESULTS

A. The CMSSM

The CMSSM is the most economical model that we study. It has only four continuous free parameters, and, consequently, it ought to be the easiest model in which to recover the ATLAS SU3 parameters.

We show the two-dimensional (2D) marginalised posterior probability density functions (pdfs) for the CMSSM's parameters for our three scans in Figure 2. Figure 2 (a) shows in effect the pdfs for the CMSSM's parameters' priors subject to physicality constraints only, because the likelihood is set equal to one. The distributions show regions where it is easier to satisfy all the physicality constraints. The log priors result in residual $1/x$ dependencies, that a priori should favour smaller parameter values. Smaller values of $m_{1/2}$ and smaller absolute values of A_0 are favoured. There is no preference for the values of $\tan\beta$ and m_0.

[5] Available at `http://kraml.web.cern.ch/kraml/comparison/`, documented in Refs. [21–24].

Parameter	Description	Prior Range	Scale
CMSSM			
m_0	Unified scalar mass	50, 1000	Log
$m_{1/2}$	Unified gaugino mass	50, 1000	Log
A_0	Unified trilinear coupling	-7000, 7000	Linear
$\tan\beta$	Ratio of Higgs vevs	2, 65	Linear
NUHM: CMSSM parameters plus:			
m_{H_d}	Higgs down-type doublet mass	50, 1000	Log
m_{H_u}	Higgs up-type doublet mass	50, 1000	Log
CMSSM-NUG: CMSSM parameters plus:			
M_1	Bino mass	50, 1000	Log
M_2	Wino mass	50, 1000	Log
M_3	Gluino mass	50, 1000	Log
MSSM			
M_2	Wino mass	1, 1000	Log
m_L	Left-handed slepton mass	100, 1000	Log
m_E	Right-handed slepton mass	100, 1000	Log
m_Q	Left-handed squark mass	100, 1000	Log
m_U	Right-handed up-type-squark mass	100, 1000	Log
m_D	Right-handed down-type-squark mass	100, 1000	Log
A_U	Up-type-quark trilinear coupling	1, 1000	Log
A_D	Down-type-quark trilinear coupling	1, 1000	Log
A_L	Lepton trilinear coupling	1, 1000	Log
m_A	Scalar Higgs mass	100, 1000	Log
μ	Higgs parameter	1, 1000	Log
$\tan\beta$	Ratio of Higgs vevs	2, 60	Linear
MSSM-NUG: MSSM parameters plus:			
M_1	Bino mass	1, 1000	Log
M_3	Gluino mass	1, 1000	Log
Nuisance			
M_t	Top quark pole mass	163.7, 178.1	Linear
$m_b(m_b)^{\overline{MS}}$	Bottom quark mass	3.92, 4.48	Linear
$\alpha_S(M_Z)^{\overline{MS}}$	Strong coupling	0.1096, 0.1256	Linear
$1/\alpha_{em}(M_Z)^{\overline{MS}}$	Reciprocal of electromagnetic coupling	127.846, 127.99	Linear

TABLE VII: The parameters that we scanned over and their prior ranges. In all the models we assumed $\mu > 0$. Note that a log scale equally weights orders of magnitude, whereas a linear scale equally weights intervals. Mass parameters and trilinear couplings are in GeV.

Figure 2 (b) shows the 2D marginalised posterior planes for the CMSSM's parameters, when the we scanned the CMSSM with simulated LHC constraints. The ATLAS SU3 point is reasonably well reconstructed for m_0 and $m_{1/2}$, though large values of m_0 are permitted. The other parameters, $\tan\beta$ and A_0, are poorly reconstructed. The sign of A_0 is ambiguous. The best fit point is not accurate — it lies away from the ATLAS SU3 value. The NS algorithm with the settings that we chose does not accurately map the profile likelihood, and, consequently, does not accurately find the best fit point. By comparing our results with a similar scan done previously in Ref. [15], we can see that our results are very similar. Our one- and two-sigma contours and our posterior means agree well with the previous results.

Figure 2 (c) shows the 2D marginalised posterior planes for the CMSSM's parameters, when we scanned the CMSSM with simulated LHC and simulated WMAP constraints. This results in a significant squeeze on m_0, with the best fit point now in line with the true value and the posterior mean. On the other hand, the best fit value of $m_{1/2}$ has increased somewhat but this is merely a reflection of the NS algorithm's poor ability to find it. We also note some tightening of $\tan\beta$. The $m_{1/2}$ and A_0 parameters show little improvement over Figure 2 (b).

Note that, compared to [15], the effect of imposing the DM density constraint is somewhat less severe. This is because we have assumed a more conservative value for the error $\sigma_{\rm CALC}$, as mentioned above.

The features presented in Figure 2 are displayed even more clearly in Figure 3 which shows the one-dimensional (1D) marginalised posterior pdfs (dash blue), as well as the profile likelihood (solid red) for the CMSSM parameters. Compared to Figure 3 (a), where the profile likelihood is set equal to one, Figure 3 (b) shows that the simulated LHC measurements restrict $m_{1/2}$ strongly, whilst restricting m_0, $\tan\beta$ and A_0 decreasingly less so. Adding the dark matter density constraint (Figure 3 (c)) mostly disfavours large m_0 and, to a lesser extent, large $\tan\beta$, but has relatively

Technical details	
`SuperBayeS` version	Adapted version 1.5
Sampling algorithm	Nested sampling
Number of processors	1
Constant efficiency mode	False
Multiple modes expected	True
Parameters for mode separation	2 (usually m_0 and $m_{1/2}$)
Maximum number of modes expected	2
Maximum number of live points	4000
Evidence tolerance factor	0.5
Sampling efficiency	2
Compilers	`ifort` and `icc`
Run time	Typically less than 3 days

TABLE VIII: The technical details of our `SuperBayeS` runs.

little effect on the other two CMSSM parameters.

Figure 4 shows the 1D marginalised posterior pdfs for the ATLAS SU3 measurable masses and mass differences for our three scans of the CMSSM. Whilst the initial ranges (Figure 4 (a)) were quite wide, Figure 4 (b) shows that the mass constraints were well recovered when the CMSSM was scanned with simulated ATLAS constraints. Like in Ref. [15], assuming the CMSSM improves the determination of the measurable masses and mass differences, that is, the derived confidence intervals are narrower than the experimental confidence intervals. This is because the geometry of the CMSSM's parameter space disfavours some combinations of masses. The simulated WMAP constraints (Figure 4 (c)), however, does not improve the recovery of the mass constraints much further. The biggest effect can be seen in the measurements of $m_{\tilde{q}} - m_{\chi}$ and $m_{\tilde{l}} - m_{\chi}$, because the masses of $\tilde{q}$ and $\tilde{l}$ depend on m_0 whose reconstruction improves by adding the information on the LSP relic density.

In summary, reconstruction of the ATLAS SU3 parameters is reasonable in the CMSSM. The parameters m_0 and $m_{1/2}$ are well reconstructed, but the reconstruction of A_0 and $\tan\beta$ is much poorer. Adding the simulated dark matter information squeezes m_0, but does not improve the recovery of the other parameters. Assuming the CMSSM narrows the confidence interval for m_{χ}.

B. The NUHM

Compared with the CMSSM, the NUHM has two additional parameters, m_{H_u} and m_{H_d}, which do not directly enter the assumed ATLAS positive end-point measurement. It is therefore interesting to investigate how their presence will affect mass reconstruction compared with the CMSSM.

In Figure 5 we show the 2D marginalised posterior planes for the NUHM's parameters for our three scans, in a similar fashion to the the CMSSM results shown above. Figure 5 (a) shows the pdfs for the NUHM's parameters' priors, because the likelihood is always set equal to one. Like the plots for the CMSSM in Figure 2 (a), with physicality constraints only, smaller values of $m_{1/2}$ and smaller absolute values of A_0 are favoured. Unlike m_0 in the CMSSM, smaller values of m_0 in the NUHM are disfavoured. There is no preference for the values of $\tan\beta$ and m_{H_u}; however, smaller values of m_{H_d} are favoured.

Figure 5 (b) shows the 2D marginalised posterior planes for the NUHM's parameters, when the we scanned the NUHM with simulated LHC constraints. The ATLAS SU3 point is reasonably well reconstructed for $m_{1/2}$, like in the CMSSM. Also, fairly large values of m_0 are permitted, but unlike in the CMSSM, small values of m_0 are also permitted. Like in the CMSSM, the other parameters, $\tan\beta$, A_0, m_{H_d} and m_{H_u} are poorly reconstructed and the sign of A_0 is ambiguous.

We can see that the reconstruction of m_0 in the NUHM is significantly poorer than it was in the CMSSM, with small values of m_0 being permitted in the NUHM. This is because the extra NUHM parameters, m_{H_d} and m_{H_u}, contribute (positively) to sfermion masses. Large values of m_{H_d} and m_{H_u} can, therefore, compensate for a small value of m_0. This results in small values of m_0 being permitted. The reconstruction of the additional NUHM parameters is also poor, especially m_{H_u}, in a way resembling the results of a global scan performed in Ref. [14].

Figure 5 (c) shows the 2D marginalised posterior planes for the NUHM's parameters, when we scanned the NUHM with simulated LHC and simulated WMAP constraints. Like in the CMSSM, there is a significant squeeze on m_0, though its reconstruction remains poor. The $\tan\beta$, A_0, m_{H_d} and m_{H_u} parameters show little improvement over Figure 5 (b).

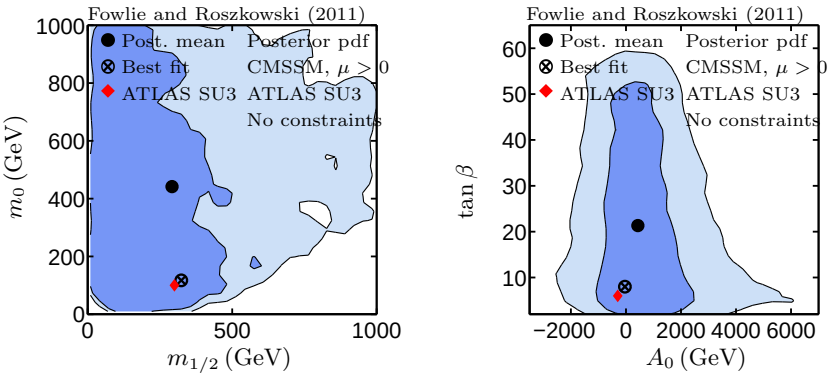

(a) CMSSM with no constraints.

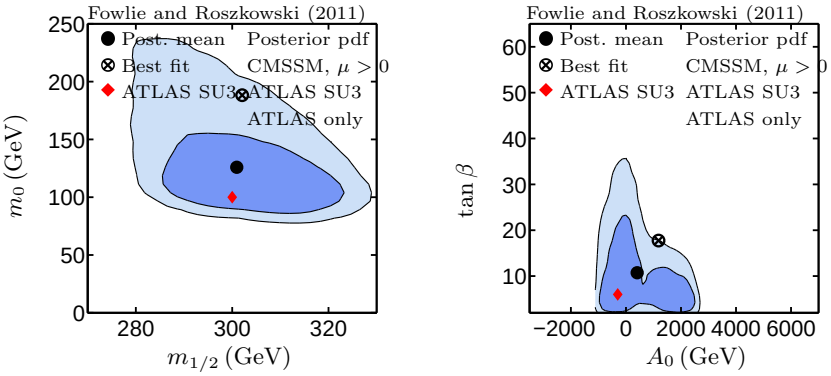

(b) CMSSM with simulated LHC constraints

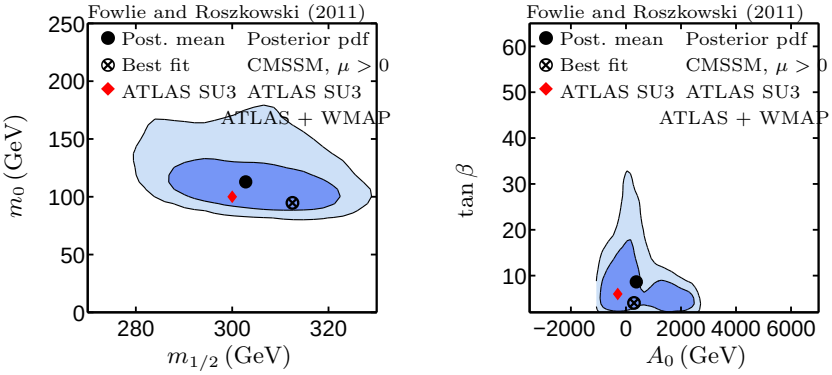

(c) CMSSM with simulated LHC and simulated WMAP constraints

FIG. 2: Marginalised posterior probability density functions, when we scanned the CMSSM with no constraints (other than those of physicality) (a), simulated LHC constraints (b), and simulated LHC and simulated WMAP constraints (c). The dark blue and light blue regions are the one-sigma and two-sigma regions respectively. The crosses on the planes are the best-fit values: the values for which χ^2 was minimised. The dots on the planes are the posterior means. The red diamonds on the planes are the ATLAS SU3 benchmark values.

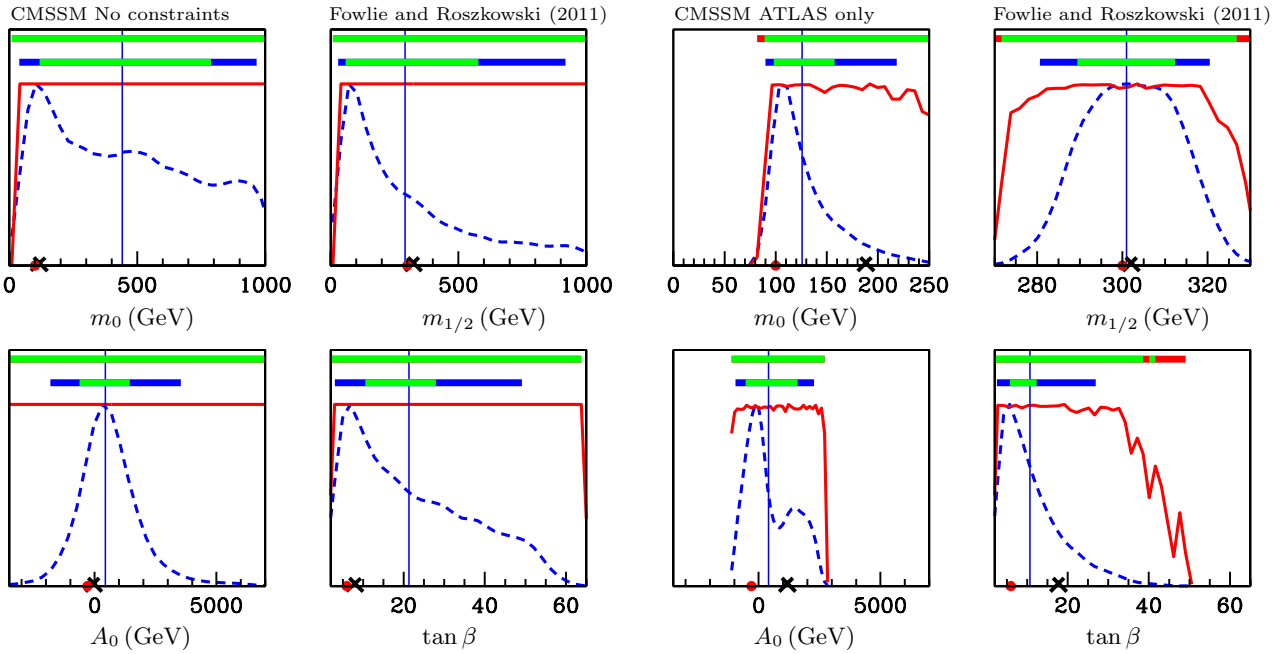

(a) CMSSM with no constraints

(b) CMSSM with simulated LHC constraints

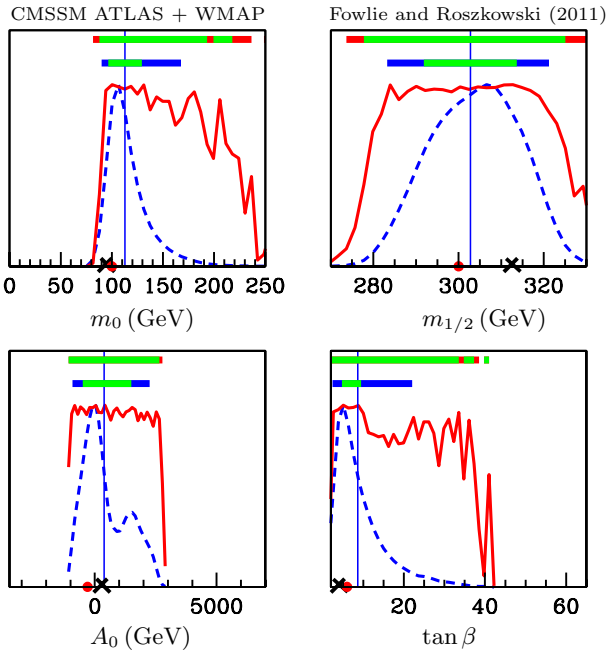

(c) CMSSM with simulated LHC and simulated WMAP constraints

FIG. 3: Marginalised posterior probability (dash blue) and profile likelihood (red) against CMSSM's parameters, when we scanned the CMSSM with no constraints (other than those of physicality) (a), simulated LHC constraints (b), and simulated LHC and simulated WMAP constraints (c). The crosses on the abscissas are the best-fit values: the values for which χ^2 was minimised. The vertical lines are the posterior means. The top and bottom blocks of colour are the one-sigma and two-sigma (68% and 95%) intervals for profile likelihood and for marginalised posterior probability respectively. The red dots on the abscissas are the ATLAS SU3 benchmark values.

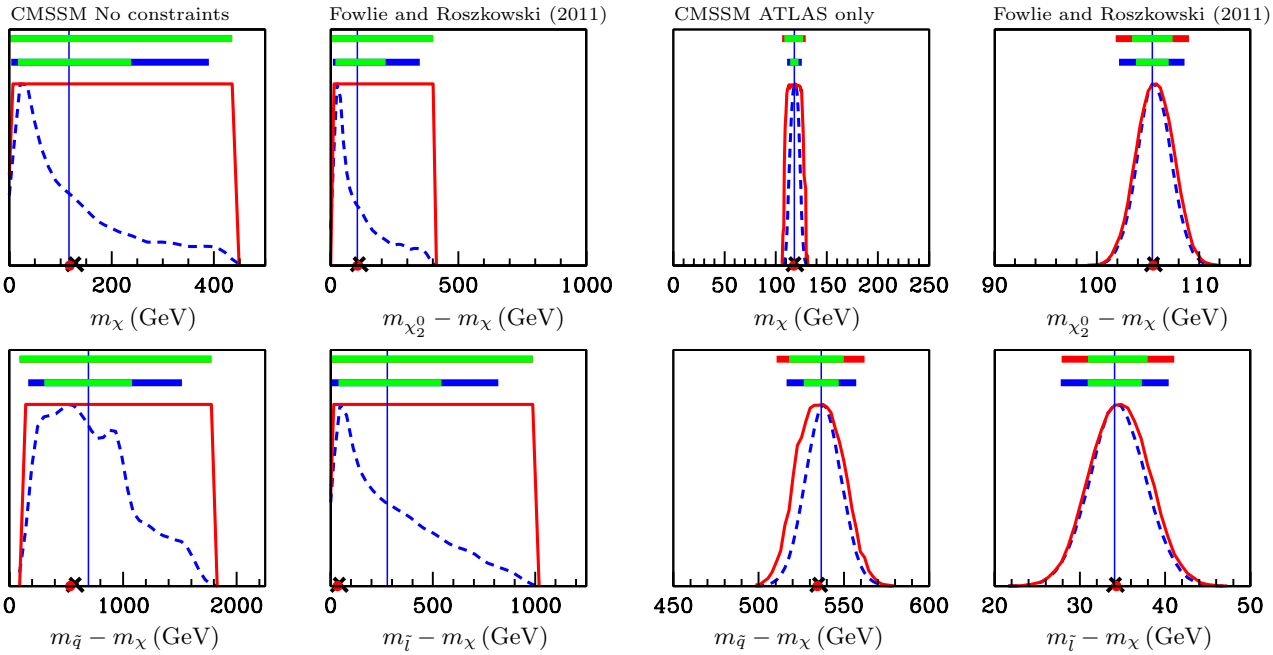

(a) CMSSM with no constraints

(b) CMSSM with simulated LHC constraints

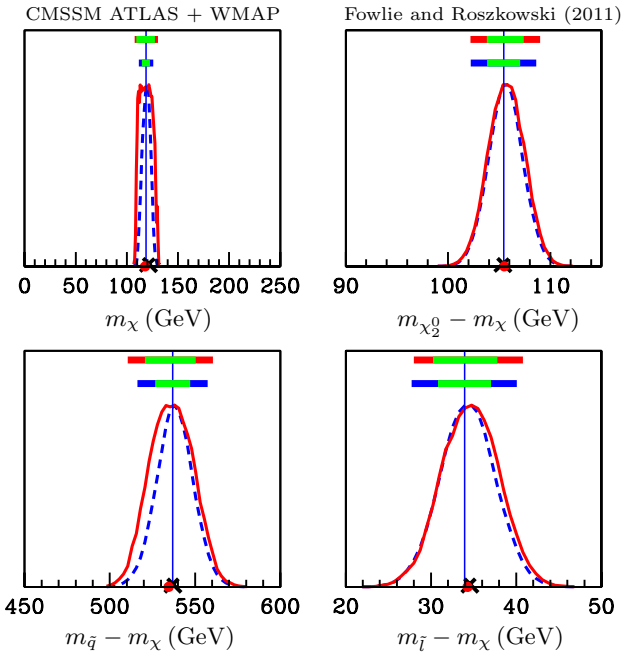

(c) CMSSM with simulated LHC and simulated WMAP constraints

FIG. 4: Marginalised posterior probability (dash blue) and profile likelihood (red) against mass constraints, when we scanned the CMSSM with no constraints (a), simulated LHC constraints (b), and simulated LHC and simulated WMAP constraints (c). The crosses on the abscissas are the best-fit values: the values for which χ^2 was minimised. The vertical lines are the posterior means. The top and bottom blocks of colour are the one-sigma and two-sigma (68% and 95%) intervals for profile likelihood and for marginalised posterior probability respectively. The red dots on the abscissas are the ATLAS SU3 benchmark values.

The marginalised pdfs for the ATLAS SU3 measurable masses and mass differences for our three scans of the NUHM are very similar to those for the CMSSM (Figure 4) and for this reason they are not shown here. Like the CMSSM's parameter space, the geometry of the NUHM's parameter space also narrows the confidence interval for m_χ.

In summary, compared with the CMSSM, parameter reconstruction in the NUHM is significantly poorer for m_0 (with much lower values now allowed), and comparable for $m_{1/2}$, A_0 and $\tan\beta$. The reconstruction of m_{H_d} and m_{H_u} is poor because the assumed ATLAS measurements basically do not depend on the Higgs sector.

C. The CMSSM-NUG

Compared with the CMSSM, the CMSSM-NUG has two additional parameters; the common gaugino mass is replaced by three independent gaugino soft mass parameters for the bino (M_1), the wino (M_2) and the gluino (M_3). Unlike the NUHM's additional parameters, the CMSSM-NUG's additional parameters do directly enter the assumed ATLAS positive end-point measurement.

In Figure 7 we show the 2D marginalised posterior planes for the CMSSM-NUG's parameters for our three scans. Figure 7 (a) shows the CMSSM-NUG's parameters' priors, because the likelihood is always set equal to one. Smaller values of M_1, M_2 and M_3 are favoured. Like in the CMSSM, smaller absolute values of A_0 are favoured and there is no preference for the values of $\tan\beta$ and m_0.

Figure 7 (b) shows the 2D marginalised posterior planes for the CMSSM-NUG's parameters, when the we scanned the CMSSM-NUG with simulated LHC constraints. The reconstruction of m_0 in the CMSSM-NUG is significantly different from its reconstruction in the CMSSM. Unlike in the CMSSM, small values of m_0 are permitted but large values of m_0 are not permitted. The shape of the m_0 and M_3 plot is different from the m_0 and $m_{1/2}$ plot in the CMSSM in Figure 2 (b). In the CMSSM-NUG, it favours smaller values of the gaugino masses. Their reconstruction is worse than the reconstruction of $m_{1/2}$ in the CMSSM in Figure 2 (b). In the CMSSM-NUG, wider ranges of M_1, M_2 and M_3 are permitted. Like in the CMSSM, $\tan\beta$ is poorly reconstructed and the sign of A_0 is ambiguous.

Unfortunately, an egregious prior effect is hampering reconstruction in the CMSSM-NUG. Figure 8 (a) shows that the CMSSM-NUG's priors favour smaller values of M_1, M_2 and M_3, and, consequently, Figure 9 (a) shows that the CMSSM-NUG's priors favour very small neutralino masses. Because of the small neutralino masses, the squark and slepton masses must be small so that the mass differences are correct. This pushes the allowed m_0 values down, so that large values are not permitted and so that small values are favoured.

The effect of adding the simulated WMAP constraint marginalised posterior planes for the CMSSM-NUG's parameters is shown in Figure 7 (c). The reconstruction of M_1, M_2 and M_3 is greatly improved over Figure 7 (b). Small values of m_0 are no longer permitted. Larger values of m_0 are preferred over Figure 7 (b), and the reconstruction of $\tan\beta$ is a bit worse than in Figure 7 (b). It appears that the stronger likelihood removes the egregious prior effect, as the plots bear similarity with Figure 2 (c). A similar conclusion can be drawn by comparing Figure 8 (b) and 8 (c) with Figure 8 (a).

Figure 9 shows the 1D marginalised posterior plots for the ATLAS SU3 measurable masses and mass differences for our three scans of the CMSSM-NUG. The plots are different from those for the CMSSM (Figure 4). Figure 9 (a) shows that the CMSSM-NUG's priors favours small lightest neutralino masses. This affects the recovery of m_χ in Figure 9 (b). The simulated WMAP constraints (Figure 9 (c)) improved the recovery of the mass constraints, though the recovery was still worse than it was in the CMSSM and the NUHM.

In contrast to the CMSSM's parameter space, the geometry of the CMSSM-NUG's parameter space does not narrow the confidence interval for m_χ. The relaxing of gaugino mass unification in the CMSSM-NUG permits combinations of masses that were previously impossible in the CMSSM.

The a priori CMSSM-NUG's prior preference for small neutralino masses (shown in Figure 9 (a)) leads, remarkably, to some tension between the LHC constraint and the WMAP constraint in the model. Generally, relative to the CMSSM's priors, the NUHM's priors favour larger relic densities and the CMSSM-NUG's priors favour smaller relic densities (though in all models small values of the relic density are favoured because of a fairly light sparticle mass spectrum involved). In the CMSSM-NUG scanned with simulated LHC constraints, because the relic density's prior favours small values, the posterior for the relic density is not centred on its ATLAS SU3 value, but below it. This creates a conflict between the simulated LHC and simulated WMAP constraints.

In summary, parameter reconstruction in the CMSSM-NUG is poorer than it was in the CMSSM, and the results are dependent on the choice of prior. Wide ranges of M_1, M_2 and M_3 are permitted in the CMSSM-NUG, but in the CMSSM, $m_{1/2}$ was tightly squeezed. Furthermore, small values of m_0, that were excluded in the CMSSM, are permitted in the CMSSM-NUG. The recovery of $\tan\beta$ and A_0 is comparable in the CMSSM-NUG and CMSSM.

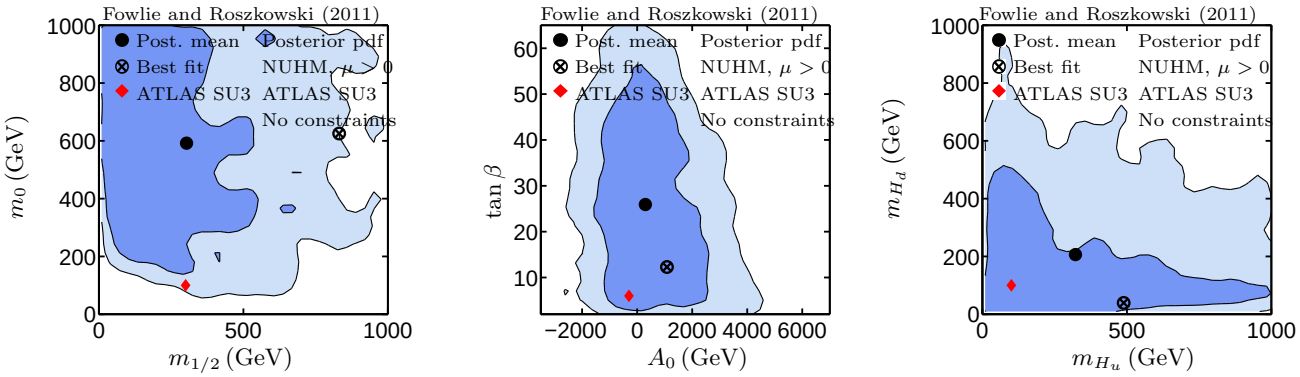

(a) NUHM with no constraints

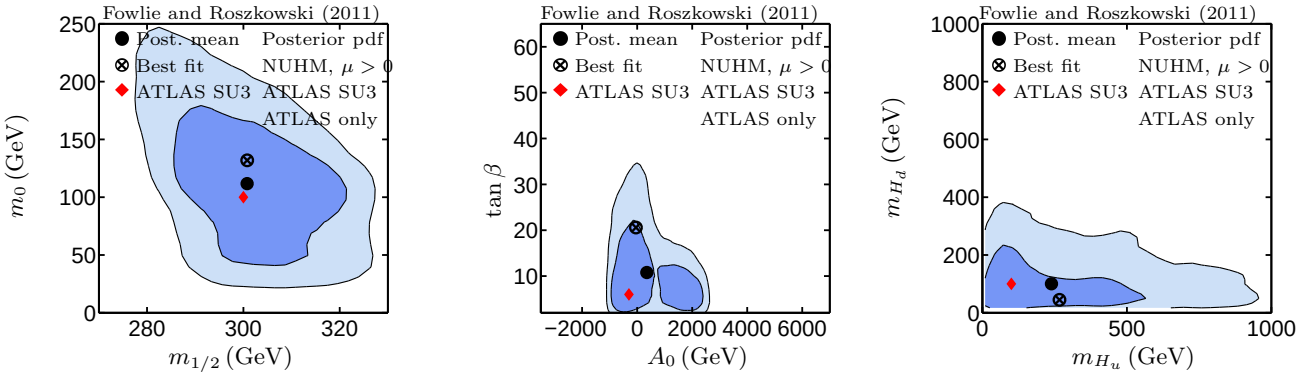

(b) NUHM with simulated LHC constraints

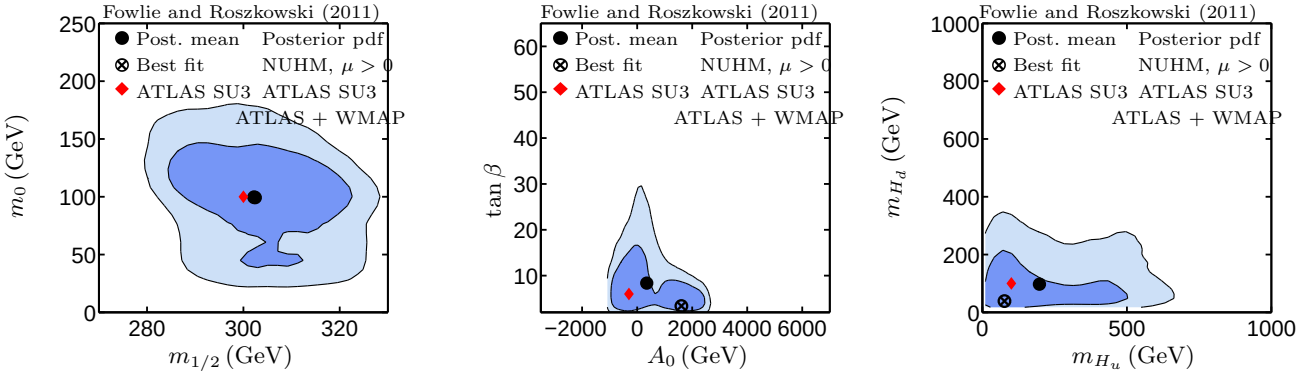

(c) NUHM with simulated LHC and simulated WMAP constraints

FIG. 5: Marginalised posterior probability planes, when we scanned the NUHM with no constraints (a), simulated LHC constraints (b), and simulated LHC and simulated WMAP constraints (c). The dark blue and light blue regions are the one-sigma and two-sigma regions respectively. The crosses on the planes are the best-fit values: the values for which χ^2 was minimised. The dots on the planes are the posterior means. The red diamonds on the planes are the ATLAS SU3 benchmark values.

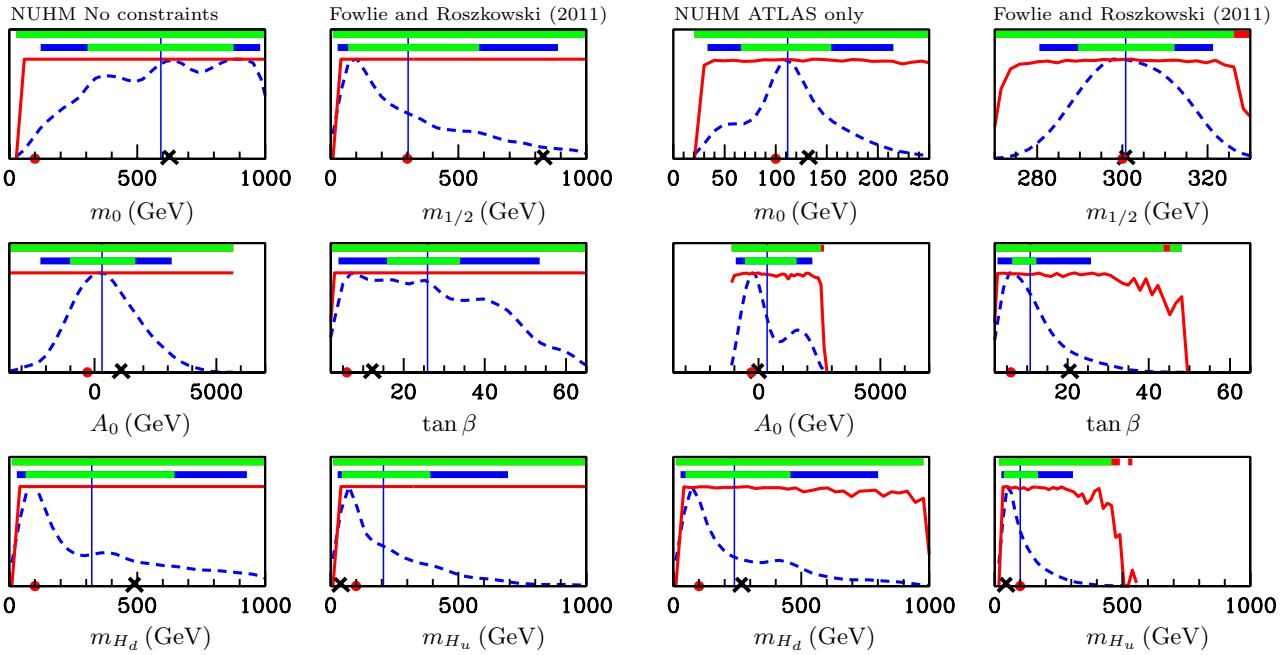

(a) NUHM with no constraints

(b) NUHM with simulated LHC constraints

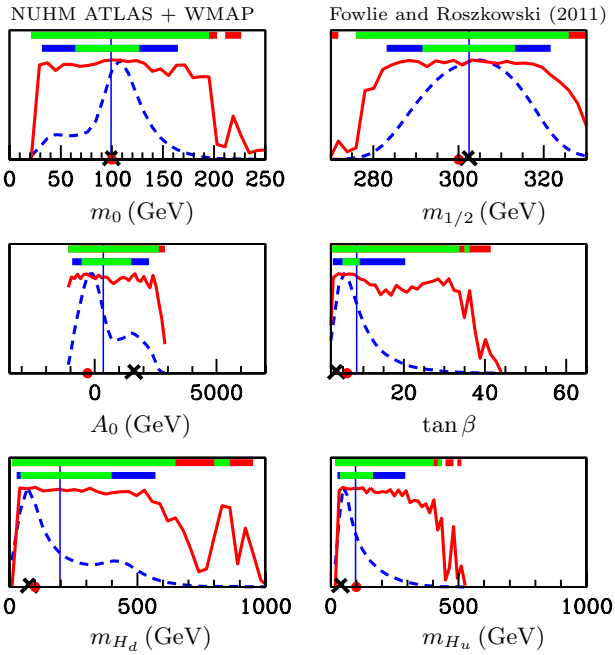

(c) NUHM with simulated LHC and simulated WMAP constraints

FIG. 6: Marginalised posterior probability (dash blue) and profile likelihood (red) against NUHM's parameters, when we scanned the NUHM with no constraints (a), simulated LHC constraints (b), and simulated LHC and simulated WMAP constraints (c). The crosses on the abscissas are the best-fit values: the values for which χ^2 was minimised. The vertical lines are the posterior means. The top and bottom blocks of colour are the one-sigma and two-sigma (68% and 95%) intervals for profile likelihood and for marginalised posterior probability respectively. The red dots on the abscissas are the ATLAS SU3 benchmark values.

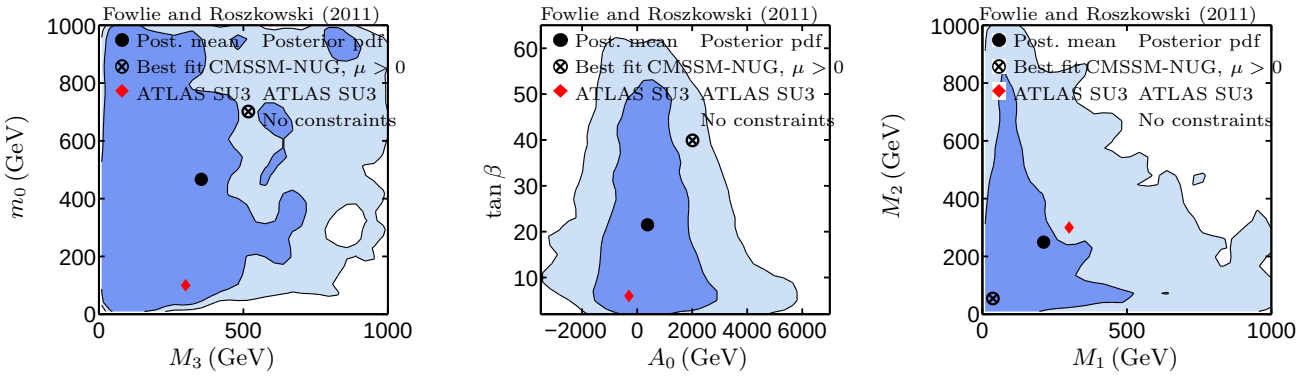

(a) CMSSM-NUG with no constraints

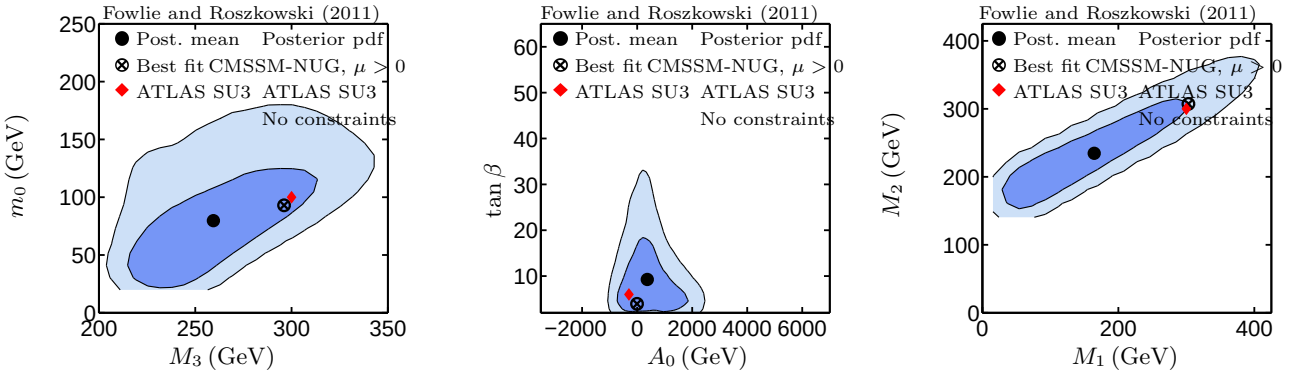

(b) CMSSM-NUG with simulated LHC constraints

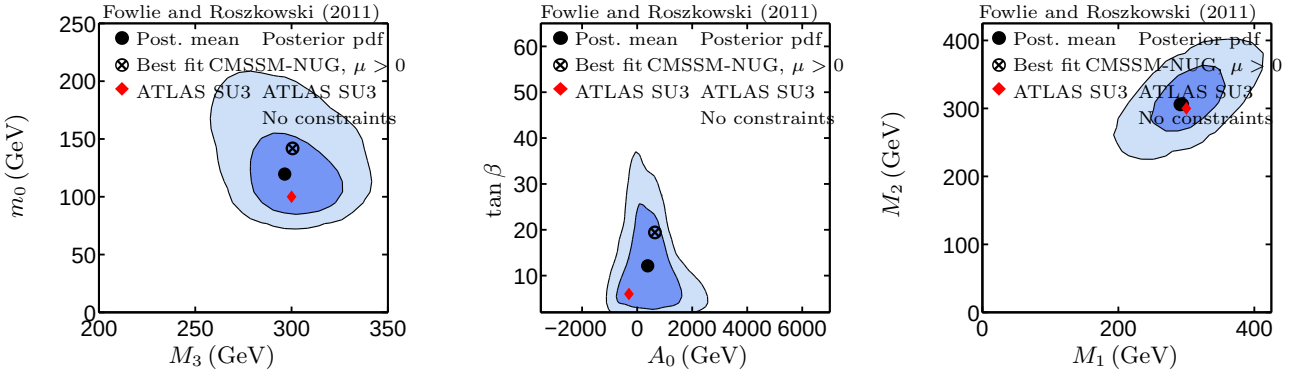

(c) CMSSM-NUG with simulated LHC and simulated WMAP constraints

FIG. 7: Marginalised posterior probability planes, when we scanned the CMSSM-NUG with no constraints (a), simulated LHC constraints (b), and simulated LHC and simulated WMAP constraints (c). The dark blue and light blue regions are the one-sigma and two-sigma regions respectively. The crosses on the planes are the best-fit values: the values for which χ^2 was minimised. The dots on the planes are the posterior means. The red diamonds on the planes are the ATLAS SU3 benchmark values.

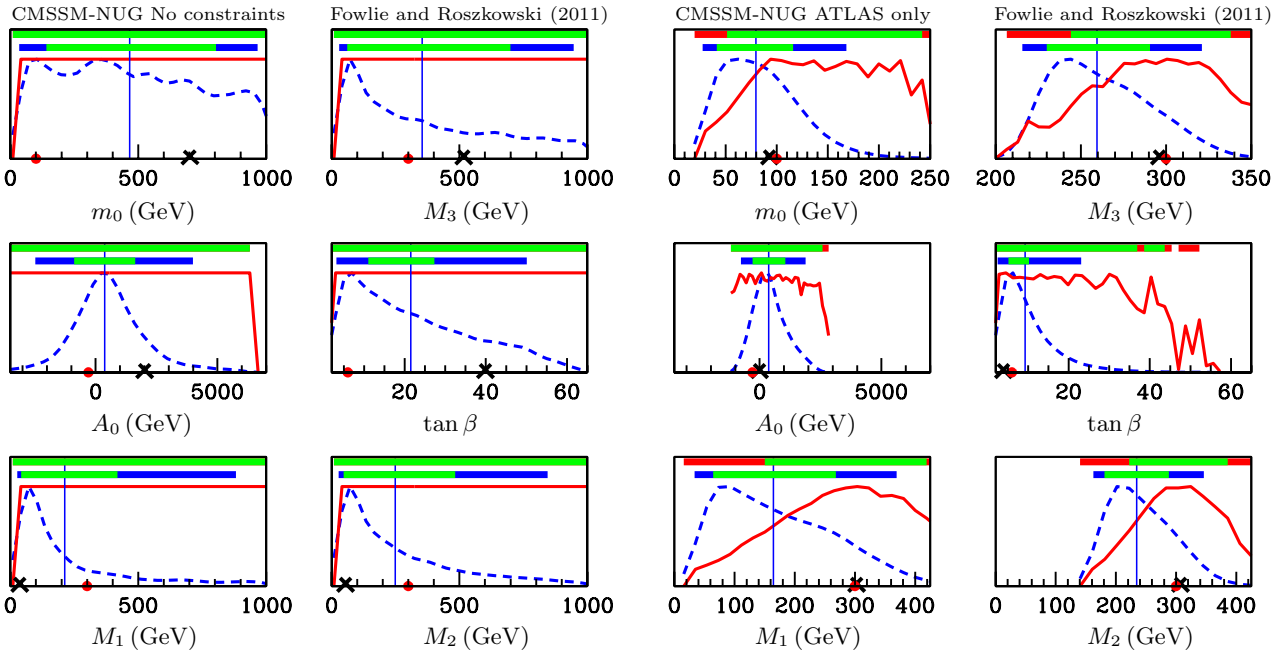

(a) CMSSM-NUG with no constraints

(b) CMSSM-NUG with simulated LHC constraints

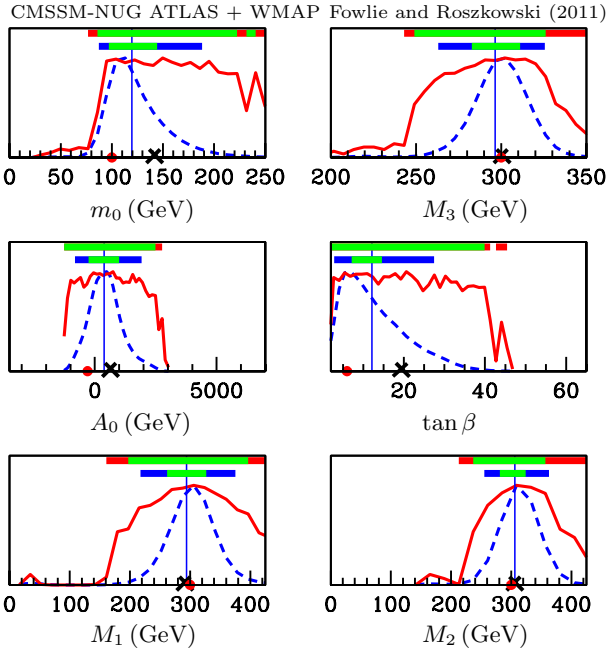

(c) CMSSM-NUG with simulated LHC and simulated WMAP constraints

FIG. 8: Marginalised posterior probability (dash blue) and profile likelihood (red) against the CMSSM-NUG's parameters, when we scanned the CMSSM-NUG with no constraints (a), simulated LHC constraints (b), and simulated LHC and simulated WMAP constraints (c). The crosses on the abscissas are the best-fit values: the values for which χ^2 was minimised. The vertical lines are the posterior means. The top and bottom blocks of colour are the one-sigma and two-sigma (68% and 95%) intervals for profile likelihood and for marginalised posterior probability respectively. The red dots on the abscissas are the ATLAS SU3 benchmark values.

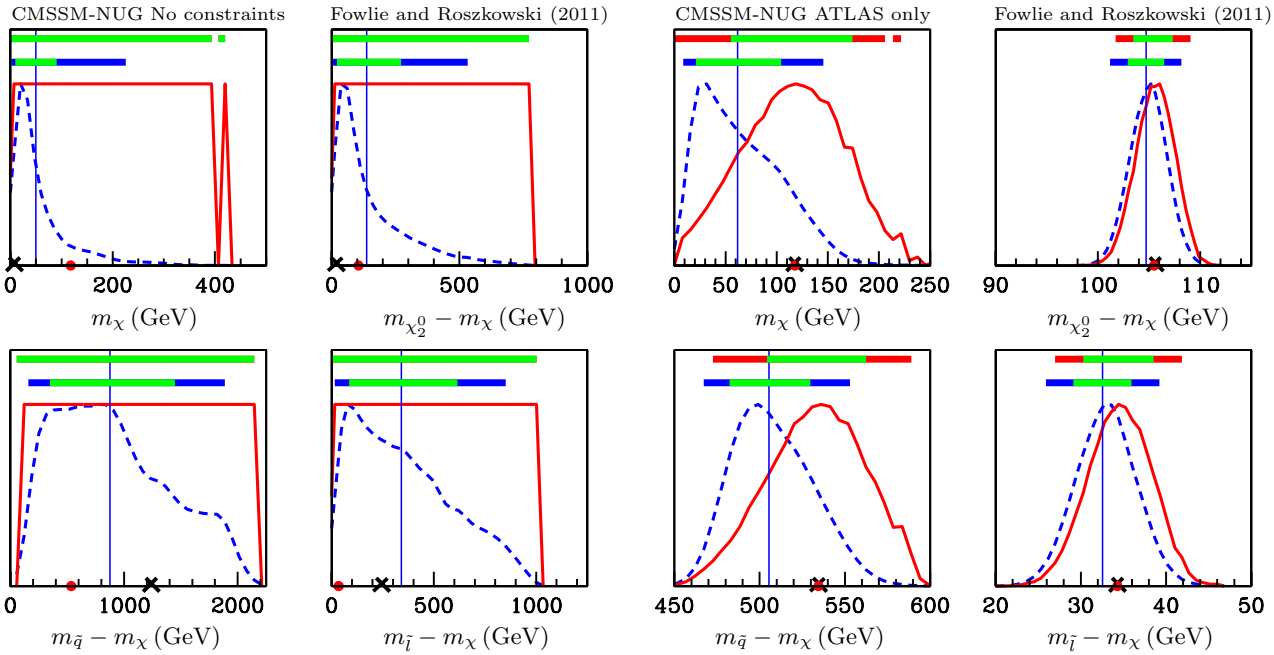

(a) CMSSM-NUG with no constraints

(b) CMSSM-NUG with simulated LHC constraints

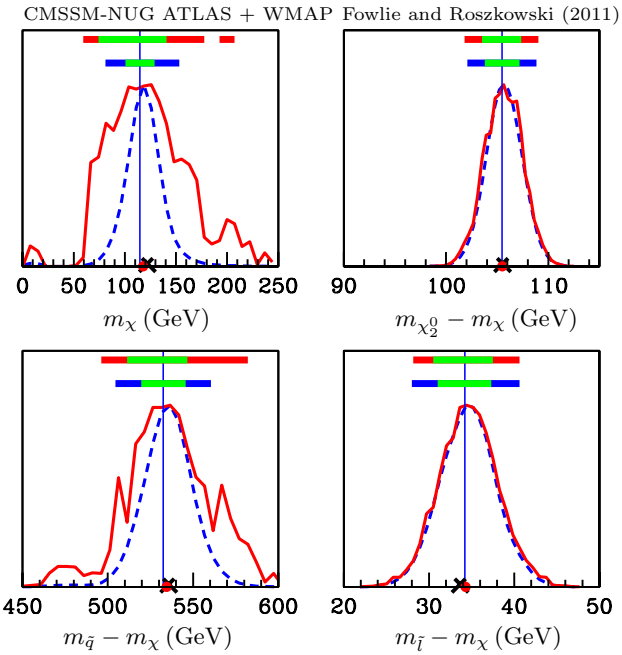

(c) CMSSM-NUG with simulated LHC and simulated WMAP constraints

FIG. 9: Marginalised posterior probability (dash blue) and profile likelihood (red) against mass constraints, when we scanned the CMSSM-NUG with no constraints (a), simulated LHC constraints (b), and simulated LHC and simulated WMAP constraints (c). The crosses on the abscissas are the best-fit values: the values for which χ^2 was minimised. The vertical lines are the posterior means. The top and bottom blocks of colour are the one-sigma and two-sigma (68% and 95%) intervals for profile likelihood and for marginalised posterior probability respectively. The red dots on the abscissas are the ATLAS SU3 benchmark values.

D. The MSSM

The MSSM that we consider is a phenomenological model defined at the EW scale with twelve parameters. Because it has much more freedom than the CMSSM, it is interesting to investigate whether its parameters can be reconstructed.

Unsurprisingly, only a few parameters were reasonably well recovered, namely M_2, μ, and m_Q. The other parameters, however, were poorly recovered in all cases. We present results for M_2, μ and m_Q, the parameters for which some reconstruction was possible, and for $\tan\beta$, to facilitate a comparison with its reconstruction in the other models.

Figure 10 shows the one-dimensional (1D) marginalised posterior pdfs (dash blue), as well as the profile likelihood (solid red) for the selection of MSSM parameters chosen above. Figure 10 (a) shows the pdfs for the MSSM's parameters' priors, because the likelihood is always set equal to one. The priors for the mass parameters show a $1/x$ shape. Smaller values of $\tan\beta$ are favoured.

Figure 10 (b) shows the one-dimensional (1D) marginalised posterior pdfs (dash blue) when we added the simulated LHC constraints. The parameters M_2, μ and m_Q are well determined, because they feature directly in the ATLAS constraints in the likelihood function. For M_2 (which to a large extent determines $m_{\chi_2^0}$) and μ the posterior means are very close to the ATLAS SU3 values. Compared to its reconstruction in the CMSSM, the reconstruction of $\tan\beta$ is poor. Large values of $\tan\beta$ are allowed, and the two-sigma confidence interval only just includes the ATLAS SU3 value. Adding the WMAP dark matter constraints (Figure 10 (c)) slightly improves the reconstruction.

Figure 11 shows the 1D marginalised posterior plots for the ATLAS SU3 measurable masses and mass differences for our three scans of the MSSM. Figures 11 (b) and 11 (c) show that the recovery of the masses in the MSSM is only slightly worse than their recovery in the CMSSM (Figure 4). The geometry of the MSSM's parameter space narrows the confidence intervals for the measurable masses and mass differences, though less so than the CMSSM's parameter space.

In summary, it seems that, because of its many free parameters, parameter reconstruction in the MSSM is difficult, though the parameters M_2, μ and m_Q were reasonably well recovered, because they feature prominently in the ATLAS SU3 mass constraints. Like the CMSSM's parameter space, the geometry of the MSSM's parameter space prohibits certain mass combinations, and, consequently, narrows the the confidence interval for m_χ.

E. The MSSM-NUG

The MSSM-NUG is a phenomenological model defined at the EW scale with fourteen parameters. Because it has much more freedom than the CMSSM and even the MSSM, it is interesting to investigate whether its parameters can be reconstructed.

Like in the MSSM, only a few parameters were reasonably well recovered, namely M_2, μ, and m_Q. Surprisingly, unlike in the MSSM, however, m_L and m_E were also reasonably well recovered. This result was not robust; it was dependent on our choice of log priors. When we repeated our scans identically, except with linear priors, the reconstruction for m_L and m_E was significantly worse. We, therefore, only present results for M_2, μ, and m_Q, the parameters for which reconstruction was robust, and for $\tan\beta$, to facilitate a comparison with its reconstruction in the other models.

Figure 12 shows the 1D marginalised posterior pdfs (dash blue), as well as the profile likelihood (solid red) for the selection of MSSM-NUG parameters chosen above. Figure 12 (a) shows the pdfs for the MSSM-NUG's parameters' priors, because the likelihood is always set equal to one. The priors show a $1/x$ shape. The is no strong preference for the value of $\tan\beta$.

Compared to the MSSM, the ATLAS constraints (Figure 12 (b)) poorly recover the parameters in the MSSM-NUG, particularly μ and $\tan\beta$. The two-sigma confidence intervals for μ and $\tan\beta$ wrongly exclude the ATLAS SU3 values. Adding the WMAP dark matter constraints (Figure 12 (c)) improves the reconstruction. Smaller values of $\tan\beta$, that are closer to the ATLAS SU3 value, are now favoured. The two-sigma confidence intervals for μ and $\tan\beta$ now include the ATLAS SU3 values. The reconstruction for M_2 is excellent; the confidence interval is narrow and the posterior mean is very close to the ATLAS SU3 value. It is likely that a prior effect, similar to the problem in the CMSSM-NUG, is removed by the simulated WMAP constraints, and, consequently, the results are greatly improved.

Figure 13 shows the 1D marginalised posterior plots for the ATLAS SU3 measurable masses and mass differences for our three scans of the MSSM. Figures 13 (b) and 13 (c) show that the recovery of the masses in the MSSM-NUG is worse than their recovery in the CMSSM and MSSM (Figures 4 and 11), but better than their reconstruction in the CMSSM-NUG (Figure 9). Like the CMSSM-NUG's priors, the MSSM-NUG's priors favour light neutralino masses. The geometry of the MSSM-NUG's parameter space slightly narrows the confidence interval for m_χ.

In summary, it seems that parameter reconstruction in the MSSM-NUG is challenging and that the results have a significant dependence on the choice of prior. Only m_Q, M_2 and μ could be reasonably well recovered with linear and

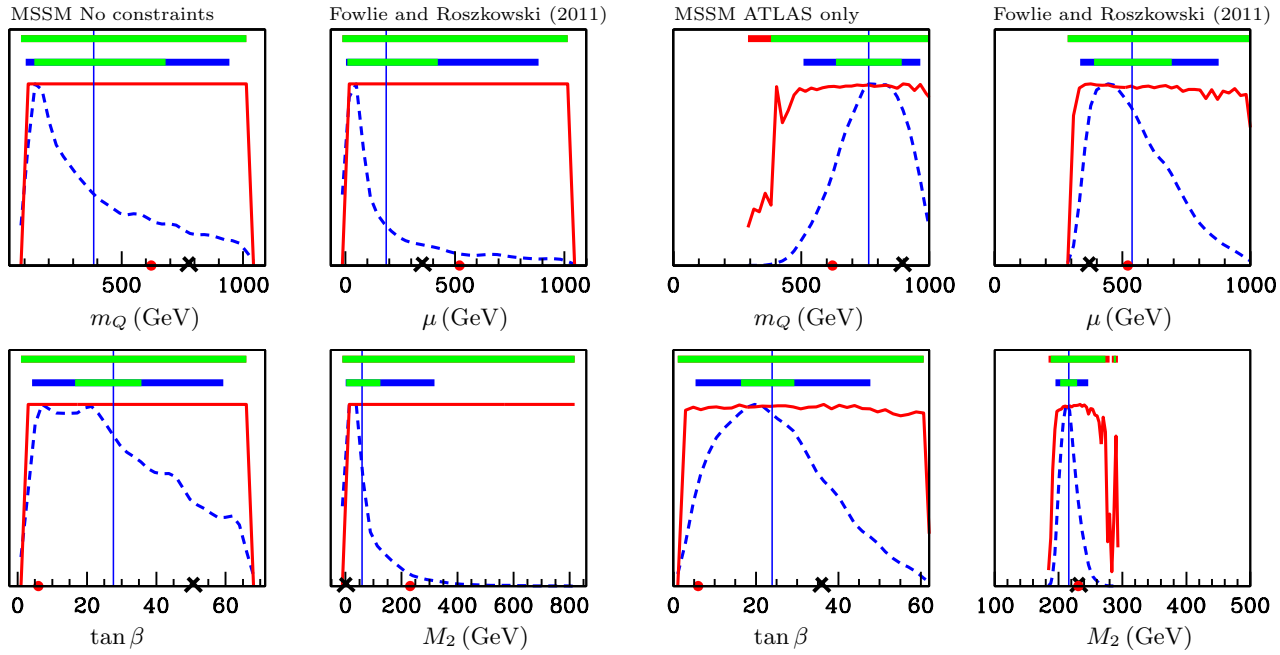

(a) MSSM with no constraints

(b) MSSM with simulated LHC constraints

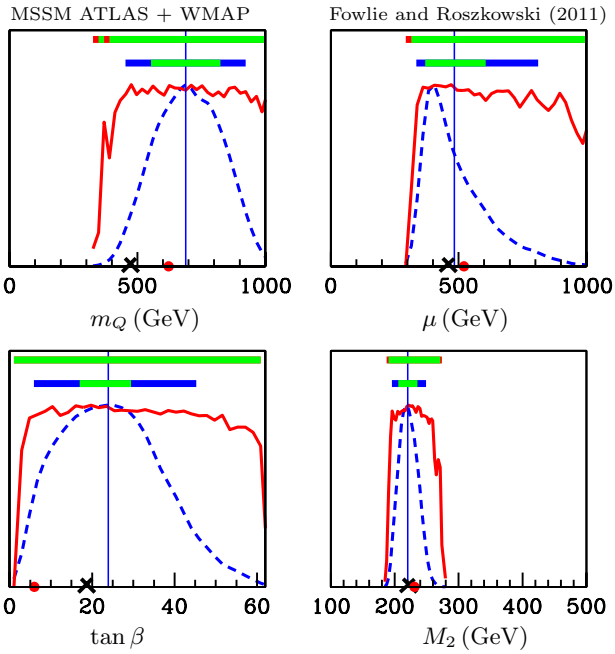

(c) MSSM with simulated LHC and simulated WMAP constraints

FIG. 10: Marginalised posterior probability (dash blue) and profile likelihood (red) against the MSSM's parameters, when we scanned the MSSM with no constraints (a), simulated LHC constraints (b), and simulated LHC and simulated WMAP constraints (c). The crosses on the abscissas are the best-fit values: the values for which χ^2 was minimised. The vertical lines are the posterior means. The top and bottom blocks of colour are the one-sigma and two-sigma (68% and 95%) intervals for profile likelihood and for marginalised posterior probability respectively. The red dots on the abscissas are the ATLAS SU3 benchmark values.

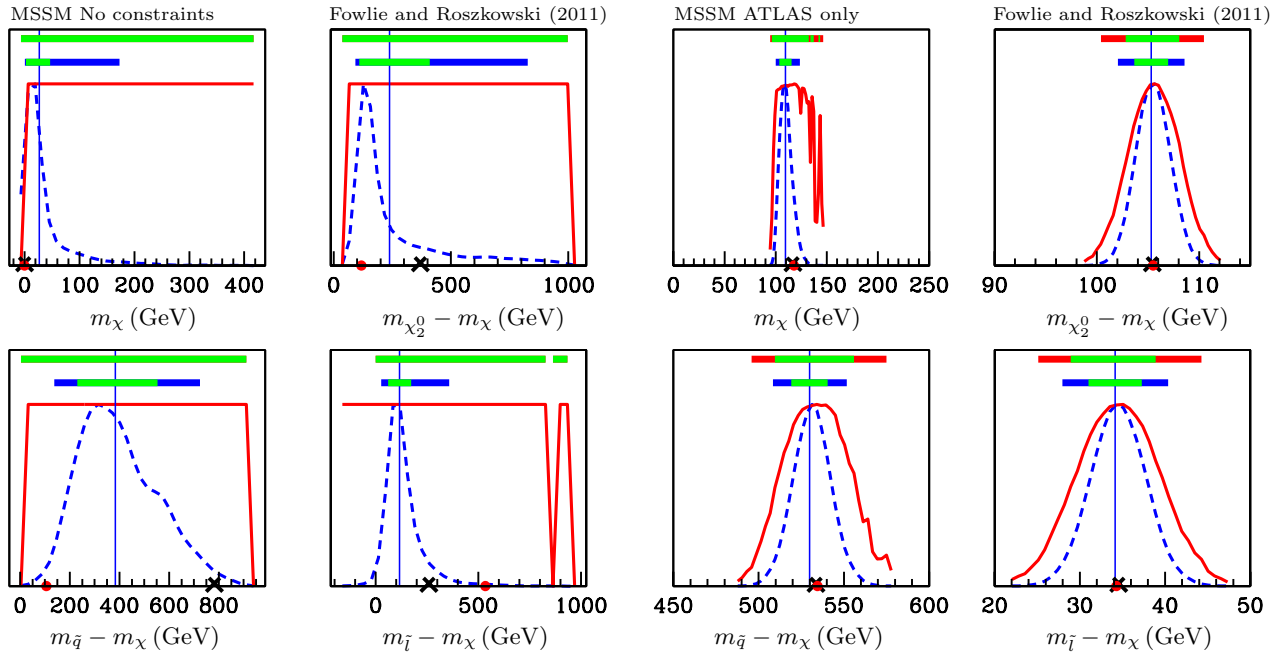

(a) MSSM with no constraints

(b) MSSM with simulated LHC constraints

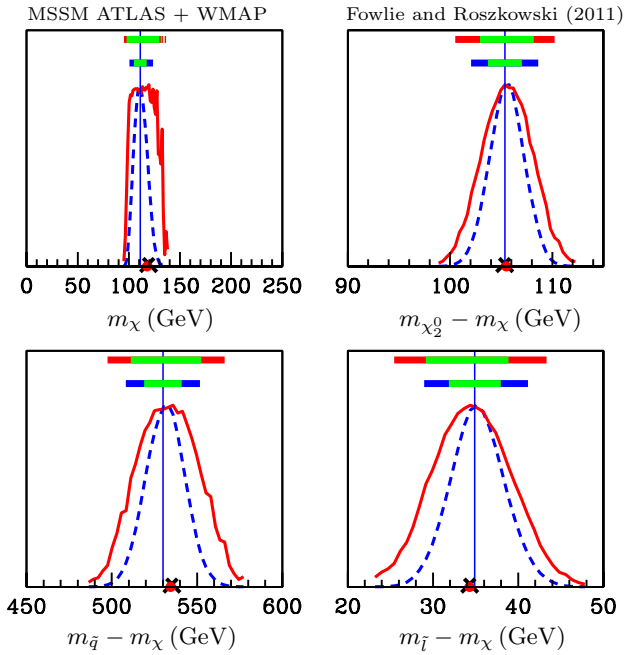

(c) MSSM with simulated LHC and simulated WMAP constraints

FIG. 11: Marginalised posterior probability (dash blue) and profile likelihood (red) against mass constraints, when we scanned the MSSM with no constraints (a), simulated LHC constraints (b), and simulated LHC and simulated WMAP constraints (c). The crosses on the abscissas are the best-fit values: the values for which χ^2 was minimised.The vertical lines are the posterior means. The top and bottom blocks of colour are the one-sigma and two-sigma (68% and 95%) intervals for profile likelihood and for marginalised posterior probability respectively. The red dots on the abscissas are the ATLAS SU3 benchmark values.

log priors. Unlike the CMSSM-NUG's parameter space, the geometry of the MSSM-NUG's parameter space slightly narrows the confidence interval for m_χ.

F. Dark Matter

The lightest neutralino plays the role of dark matter (DM). We can calculate its relic density and the rate at which we expect DM particles to be detected.

First, Figure 14 shows the 1D marginalised posterior (blue dash) for the relic density $\Omega_\chi h^2$, when we scanned the CMSSM, the NUHM, the CMSSM-NUG, and the MSSM with simulated LHC constraints. The distribution is reasonably well peaked close to the assumed correct value of 0.2332 (red dot) in the CMSSM, the NUHM and even the MSSM, although in the last case the confidence interval is much wider. In the CMSSM-NUG the reconstruction of $\Omega_\chi h^2$ is very poor because of the tension between the LHC constraint and the WMAP constraint in the model mentioned above. The case of the MSSM-NUG (not shown) looks similar to the MSSM plot. For comparison, we show (solid red) the profile likelihood curves for each case.

Turning next to direct detection, Figure 15 shows the 2D marginalised posterior planes for the neutralino mass and the spin-independent cross section on a proton σ_p^{SI}, when we scanned the CMSSM, the NUHM, the CMSSM-NUG, and the MSSM with simulated LHC and simulated WMAP constraints. The ATLAS SU3 values are well recovered in the CMSSM (Figure 15 (a)) and the NUHM (Figure 15 (b)). The ATLAS SU3 values are poorly recovered in the CMSSM-NUG (Figure 15 (c)). It is likely that this results from the poor recovery of m_χ in the CMSSM-NUG. The recovery in the MSSM (Figure 15 (d)) is worse than it is in the CMSSM and the NUHM, but better than it is in the CMSSM-NUG. The case of the MSSM-NUG (not shown) looks similar to the MSSM plot. In particular, the constraint on m_χ is only slightly worse than in the MSSM and is much better than in the CMSSM-NUG.

G. Comparison

In Figures 16 and 17 we compare the reconstruction in all five models, by plotting the various parameters' posterior means and two-sigma (95%) confidence intervals, when we scanned the models with simulated LHC and simulated WMAP constraints. We see that the two-sigma confidence intervals almost always include, and that the posterior means are always close to, the ATLAS SU3 value. The exception is that the two-sigma region for $\tan\beta$ in the MSSM (Figure 16 (d)) basically excludes the ATLAS SU3 value, whilst in the MSSM-NUG it barely allows it. Generally, the ranges of $\tan\beta$ are on the high side and not well reconstructed. The parameter A_0 is poorly reconstructed in all of the models.

The reconstruction of the ATLAS measurable masses and mass differences (Figure 17) is similar in all five models, apart from the reconstruction of m_χ, which varies between the models. The two-sigma confidence intervals for m_χ in the CMSSM and in the NUHM are similar, but the two-sigma confidence interval for m_χ in the CMSSM-NUG is much wider than it is in the other models. In the MSSM and MSSM-NUG, the two-sigma confidence interval for m_χ is slightly wider than it is in CMSSM, but narrower than it is in the CMSSM-NUG. The geometry of the CMSSM-NUG's parameter space does not forbid certain combinations of neutralino masses, resulting in a large confidence interval for m_χ.

H. Evidence

We consider whether the simulated LHC constraints or the combination of simulated LHC and simulated WMAP constraints can distinguish between the CMSSM, the NUHM and the CMSSM-NUG. The evidence[6] for each model is listed in Table IX, which also shows odds ratios; ratios of the evidence for different models. The Jefferey's scale is a subjective scale for assessing whether an odds ratio is significant. The CMSSM and the NUHM are statistically indistinguishable in all cases, the slight preference for the NUHM is not significant according to Jefferey's scale. The NUHM's extra parameters improve the fit enough to negate the penalty for having a greater prior volume.

[6] The evidence is a measure of how well and how economically a model agrees with some data. It is given by $\mathcal{Z}(D) = \int \mathcal{L}(D|H)\pi(H)dm_1 dm_2 \ldots dm_N$; see Ref. [15] for more details.

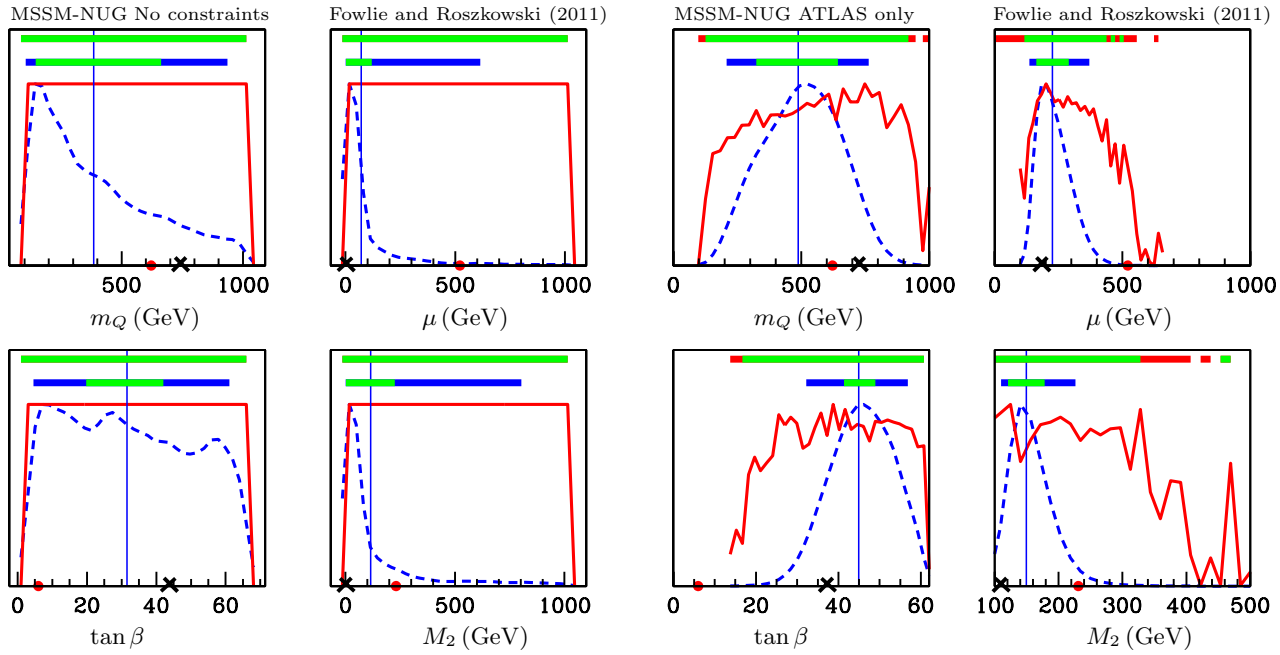

(a) MSSM-NUG with no constraints

(b) MSSM-NUG with simulated LHC constraints

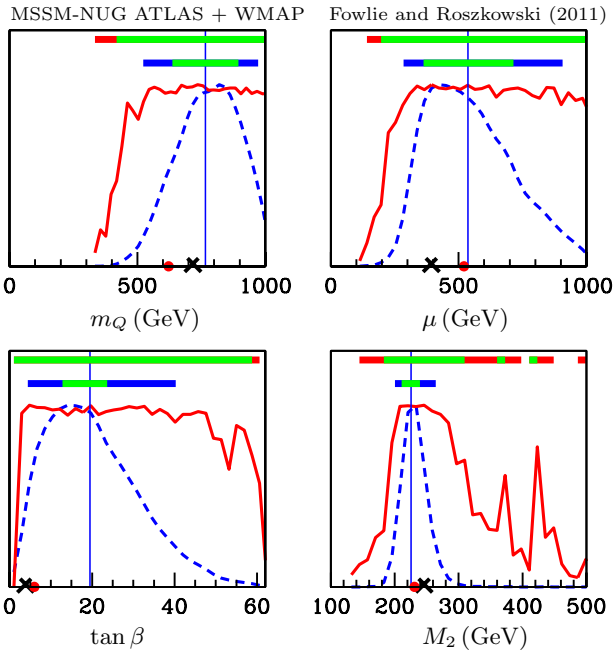

(c) MSSM-NUG with simulated LHC and simulated WMAP constraints

FIG. 12: Marginalised posterior probability (dash blue) and profile likelihood (red) against the MSSM-NUG's parameters, when we scanned the MSSM-NUG with no constraints (a), simulated LHC constraints (b), and simulated LHC and simulated WMAP constraints (c). The crosses on the abscissas are the best-fit values: the values for which χ^2 was minimised. The vertical lines are the posterior means. The top and bottom blocks of colour are the one-sigma and two-sigma (68% and 95%) intervals for profile likelihood and for marginalised posterior probability respectively. The red dots on the abscissas are the ATLAS SU3 benchmark values.

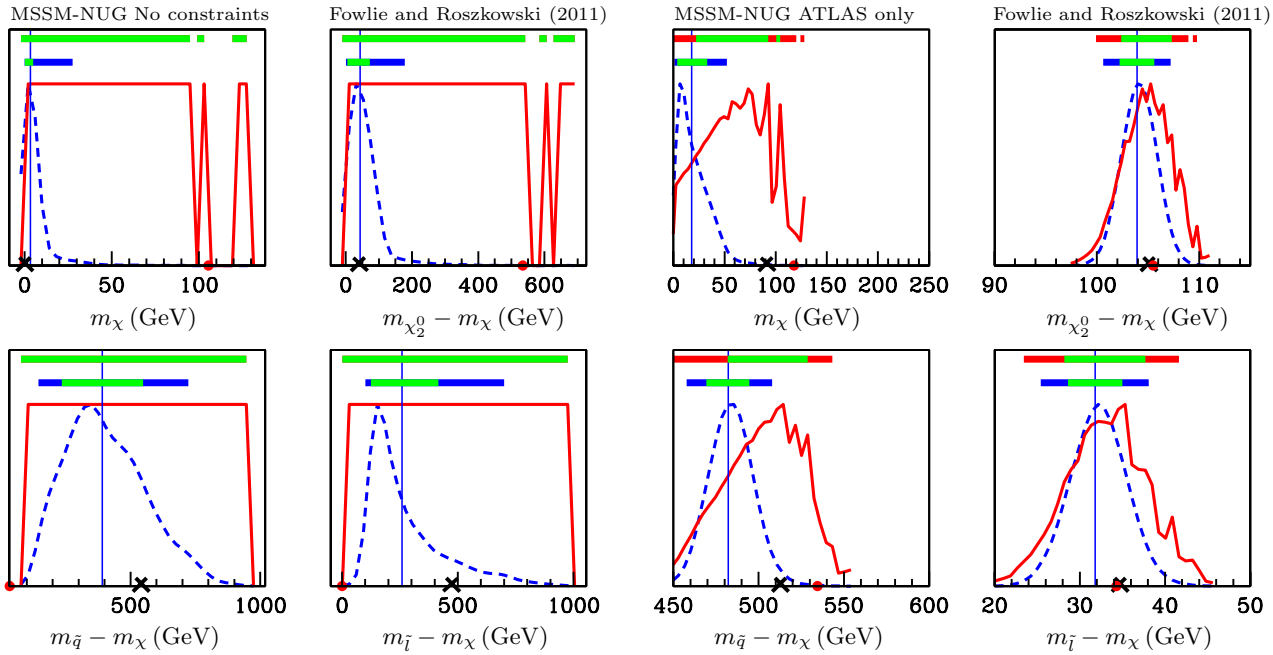

(a) MSSM-NUG with no constraints

(b) MSSM-NUG with simulated LHC constraints

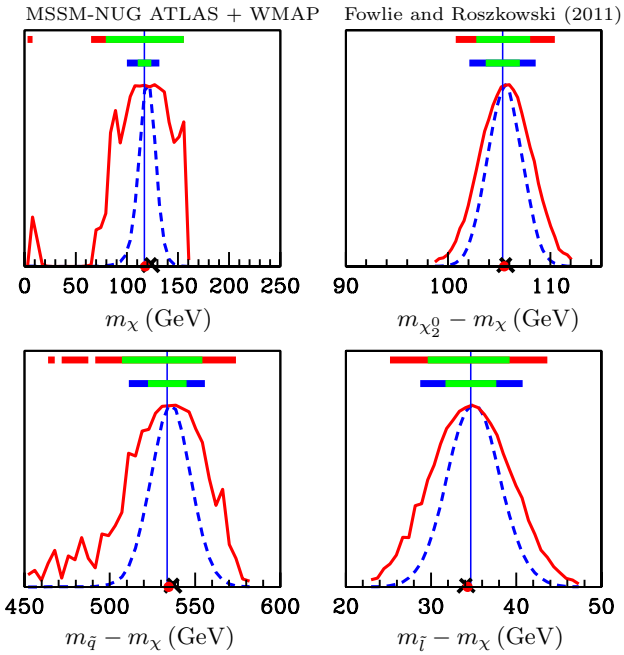

(c) MSSM-NUG with simulated LHC and simulated WMAP constraints

FIG. 13: Marginalised posterior probability (dash blue) and profile likelihood (red) against mass constraints, when we scanned the MSSM-NUG with no constraints (a), simulated LHC constraints (b), and simulated LHC and simulated WMAP constraints (c). The crosses on the abscissas are the best-fit values: the values for which χ^2 was minimised. The vertical lines are the posterior means. The top and bottom blocks of colour are the one-sigma and two-sigma (68% and 95%) intervals for profile likelihood and for marginalised posterior probability respectively. The red dots on the abscissas are the ATLAS SU3 benchmark values.

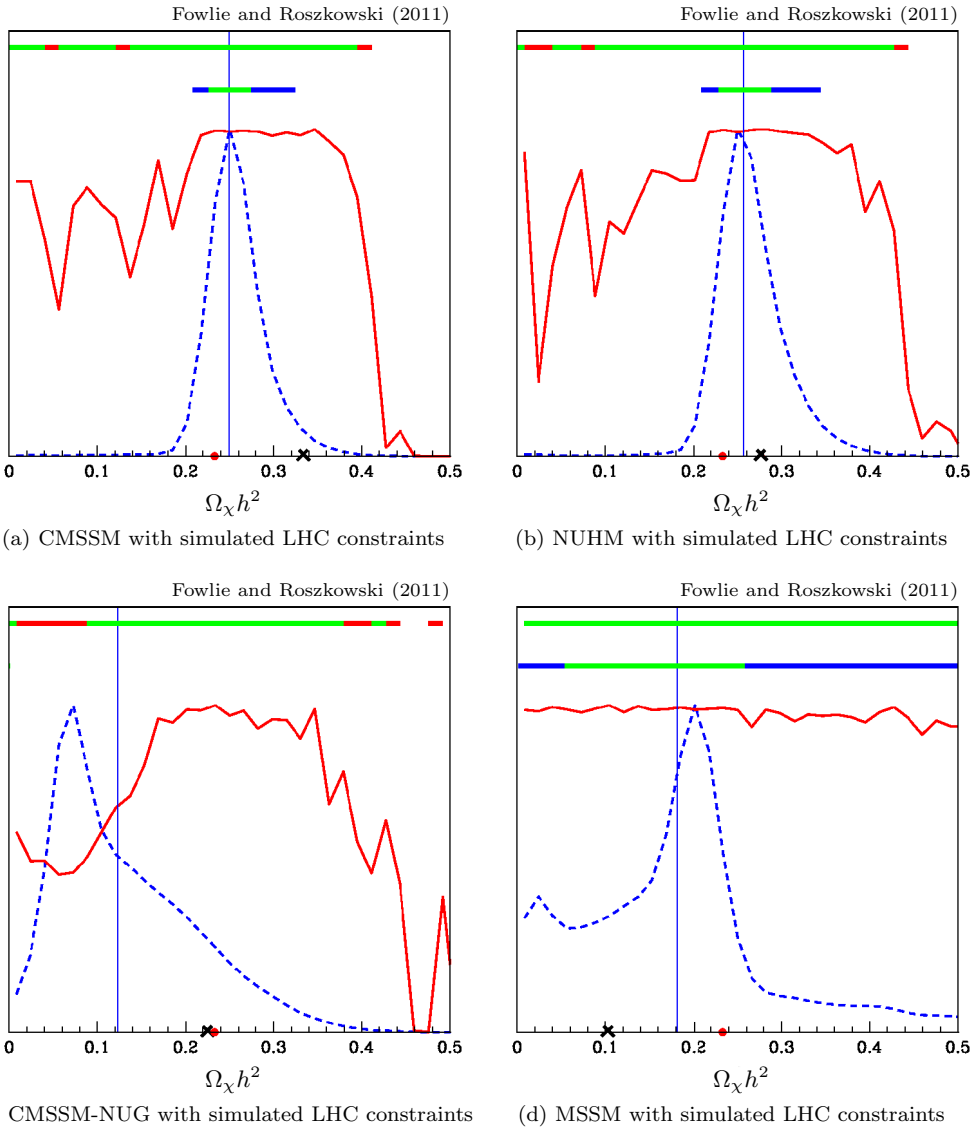

(a) CMSSM with simulated LHC constraints

(b) NUHM with simulated LHC constraints

(c) CMSSM-NUG with simulated LHC constraints

(d) MSSM with simulated LHC constraints

FIG. 14: Marginalised posterior probability (dash blue) and profile likelihood (red) of the neutralino relic density, when we scanned the CMSSM (a), the NUHM (b), the CMSSM-NUG (d) and the MSSM (d). The crosses on the abscissas are the best-fit values: the values for which χ^2 was minimised. The vertical lines are the posterior means. The top and bottom blocks of colour are the one-sigma and two-sigma (68% and 95%) intervals for profile likelihood and for marginalised posterior probability respectively. The red dots on the abscissas are the ATLAS SU3 benchmark values.

The CMSSM and the NUHM are both significantly preferred to the CMSSM-NUG in all cases. The simulated LHC constraints and our models' priors show a significant preference for the CMSSM and the NUHM over the CMSSM-NUG. The CMSSM-NUG's extra parameters are not economical; they dilute the regions of parameter space that agree with the constraints, without improving the fit.

A caveat is in order: these results are not entirely robust. We repeated our calculations, identically, except that we used linear priors, rather than log priors. A substantial preference for the CMSSM over the NUHM emerged when the evidence was calculated with simulated LHC and simulated WMAP data, due to the larger number of free parameters in the NUHM and consequently larger volume effect. The CMSSM-NUG was still significantly disfavoured in all cases.

Constraints	Natural log Evidence	CMSSM	NUHM	CMSSM-NUG
CMSSM				
Simulated LHC	-8.91 ± 0.04	1	1.06	0.02
Simulated LHC and simulated WMAP	-9.35 ± 0.04	1	1.03	0.01
NUHM				
Simulated LHC	-8.85 ± 0.04	0.94	1	0.02
Simulated LHC and simulated WMAP	-9.32 ± 0.04	0.97	1	0.01
CMSSM-NUG				
Simulated LHC	-12.70 ± 0.05	44.26	47.00	1
Simulated LHC and simulated WMAP	-14.47 ± 0.07	167.34	172.43	1

TABLE IX: The Bayesian evidence for the models that we scanned with log priors. The final three columns are odds ratios; ratios of the models' evidences. The evidences for the models in the headings of the columns are the numerators and the evidences for the models in the headings of the rows are the denominators in the ratios. An odds ratio of greater than one indicates that, for a given model (row) the model in the heading of the column is preferred over the other models (columns).

I. Choice of priors

We investigated whether our results were robust, that is, whether they were dependent on our choice of log priors, rather than linear priors. The results for the CMSSM-NUG, MSSM-NUG and for the evidences were not entirely robust. In particular, the models without gaugino mass unification (the CMSSM-NUG and MSSM-NUG) were dependent on our choice of prior.

The prior problems in the CMSSM-NUG and MSSM-NUG could have been caused by a volume effect in the log priors. Log priors equally weighted orders of magnitude. In the CMSSM's log priors, before physicality conditions were imposed, there was a 0.625 chance that the $m_{1/2}$ parameter would lie between 100 GeV and 1000 GeV. In the CMSSM-NUG's log priors, the chance that M_1 and M_2 both lay between 100 GeV and 1000 GeV was $0.625^2 = 0.391$. In other words, the fraction of log prior space in which either M_1 or M_2 is small in the CMSSM-NUG is greater than the fraction of log prior space in which $m_{1/2}$ is small in the CMSSM. Because the neutralinos' masses increase with the gaugino masses, this would lead to a prior preference for light neutralinos in the CMSSM-NUG. An identical argument can be applied to the MSSM-NUG.

The CMSSM had very little prior dependence; the results for log and linear priors were statistically indistinguishable. The NUHM's additional parameters, m_{H_u} and m_{H_d}, showed a strong prior dependence, though the results for the other parameters were indistinguishable. Of the MSSM's parameters, only the trilinear terms had a strong prior dependence. This is unsurprising, because these parameters were poorly constrained by the likelihood. The results for the CMSSM-NUG had a strong dependence on the choice of prior; the results for log priors and linear priors were different. Though this dependence was removed by the simulated WMAP data. Unsurprisingly, because it has so much freedom and is so poorly constrained by the likelihood function, the MSSM-NUG had the strongest prior dependence. It seems that the assumption of gaugino mass unification is critical; without this assumption, CMSSM and MSSM have too much freedom to be constrained by the simulated data.

The prior is information that is known before the inference. We, unfortunately, had an in-articulated prior preference for very small neutralino masses in the CMSSM-NUG and MSSM-NUG, to which we were oblivious, that were in conflict with the ATLAS SU3 sparticle mass spectrum. This is a pitfall of Bayesian statistics; the priors that you choose for the model parameters can result in unexpected and unwanted preferences for some parameters, especially when the likelihood is weakly constraining.

V. CONCLUSIONS

We have analysed the prospects of reconstructing the ATLAS SU3 benchmark point in the framework of several low-energy SUSY models with a Bayesian approach, assuming numerical information about masses and mass differences from a hypothetical positive end-point measurement by ATLAS but otherwise making a Gaussian approximation, following the method developed in Ref. [15].

As a preliminary step, in each model we delineated the ranges of the parameters that were favoured by requiring physical solutions (and that the neutralino was the LSP) alone. Next, we showed that a hypothetical ATLAS measurement would allow one to significantly constrain the common gaugino mass parameter $m_{1/2}$ and, to a lesser degree, the scalar mass parameter m_0 in models with gaugino mass unification (the CMSSM and the NUHM), though

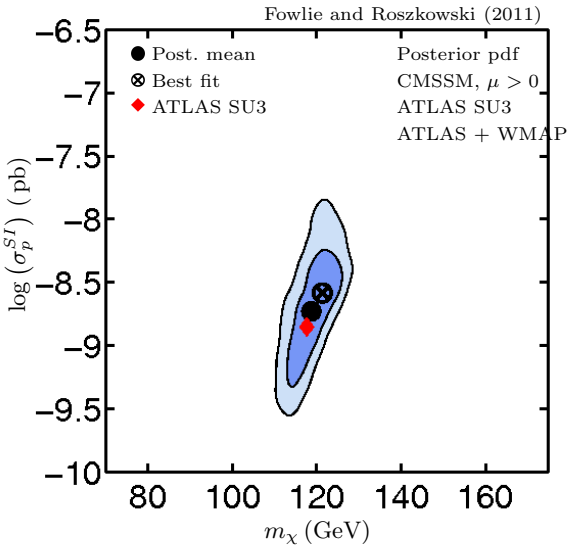

(a) CMSSM with simulated LHC and simulated WMAP constraints

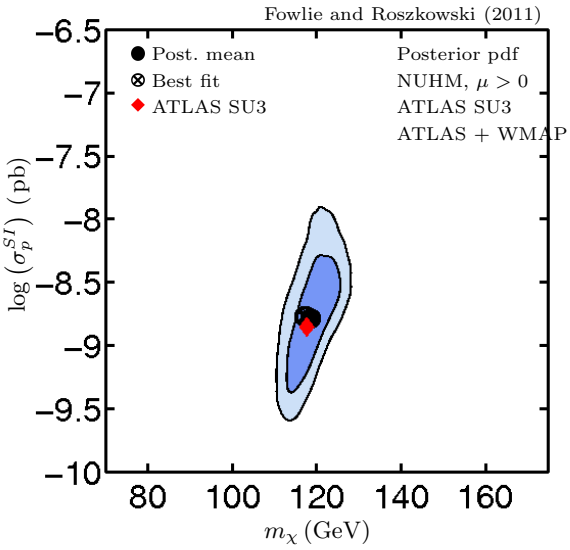

(b) NUHM with simulated LHC and simulated WMAP constraints

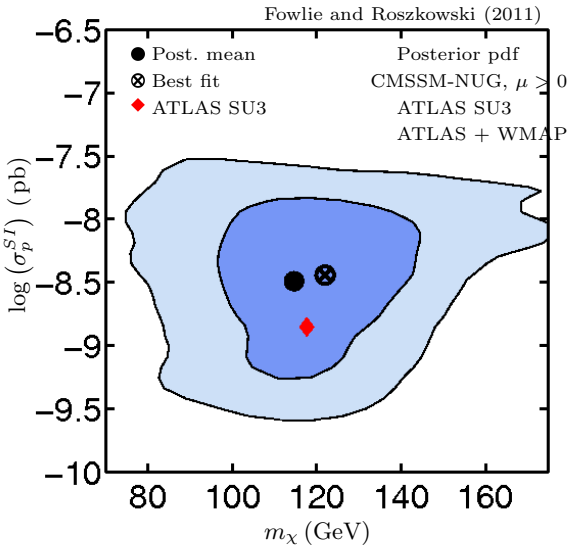

(c) CMSSM-NUG with simulated LHC and simulated WMAP constraints

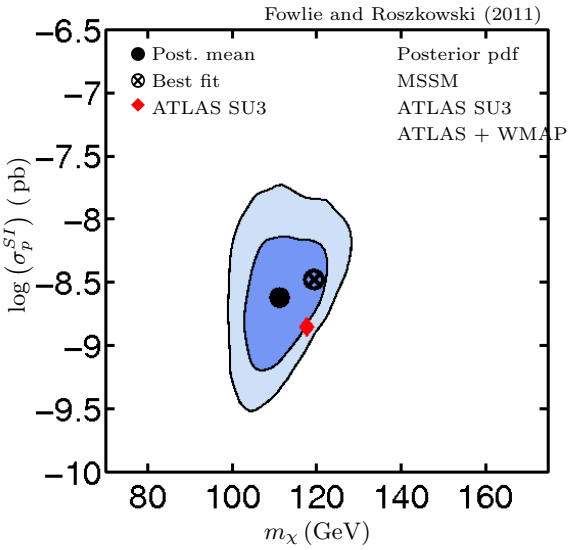

(d) MSSM with simulated LHC and simulated WMAP constraints

FIG. 15: Marginalised posterior probability planes relevant to direct detection experiments, when we scanned the CMSSM (a), the NUHM (b), the CMSSM-NUG (c), and the MSSM (d). The dark blue and light blue regions are the one-sigma and two-sigma regions respectively. The crosses on the planes are the best-fit values: the values for which χ^2 was minimised. The dots on the planes are the posterior means. The red diamonds on the planes are the ATLAS SU3 benchmark values.

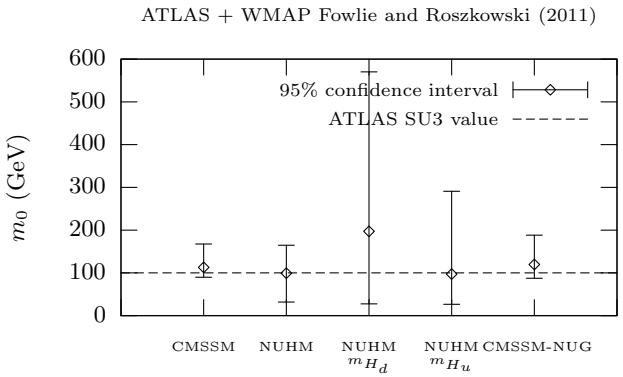

(a) m_0 reconstruction, with simulated LHC and simulated WMAP constraints

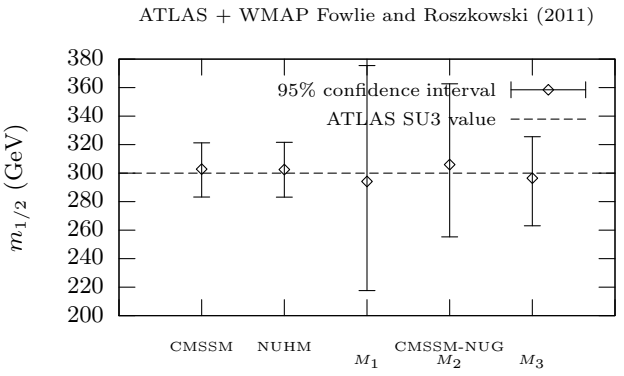

(b) $m_{1/2}$ reconstruction, with simulated LHC and simulated WMAP constraints. The parameters M_1, M_2 and M_3 are the three independent gaugino soft masses that replace $m_{1/2}$ in the CMSSM-NUG.

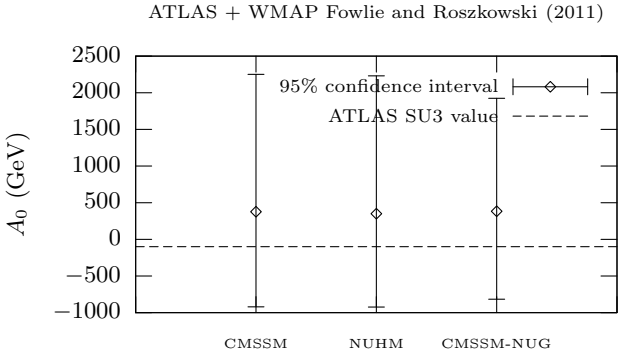

(c) A_0 reconstruction, with simulated LHC and simulated WMAP constraints

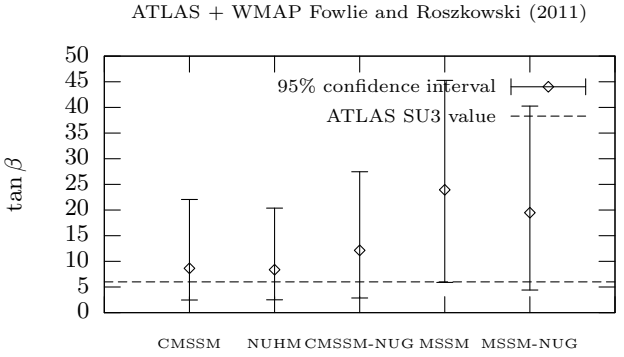

(d) $\tan\beta$ reconstruction, with simulated LHC and simulated WMAP constraints

FIG. 16: The two-sigma (95%) confidence intervals and posterior means for m_0 (a), $m_{1/2}$ (b), A_0 (c) and $\tan\beta$ (d).

in the other models the situation is much more mixed. In the future, reconstructing $\tan\beta$ will be challenging and reconstructing A_0 will be almost impossible, with even its sign remaining ambiguous in our analysis. Adding the relic density of neutralino dark matter to the likelihood improves parameter reconstruction in the unified models, especially for m_0, but there is much less improvement in the relaxed models. The assumption of gaugino mass unification seems critical to parameter reconstruction; relaxing this assumption leads to a much poorer determination of the model parameters, the "directly" measured masses and mass differences, the relic density of the neutralino and the elastic spin-independent cross section σ_p^{SI}.

In our analysis we used a log prior for all parameters other than $\tan\beta$ and A_0 (and the nuisance parameters). We did, however, test the prior dependence of our results, by repeating our analysis with a linear (flat) prior for all the parameters. We confirmed that the CMSSM has very little prior dependence [15] but we found that generally the other models have a rather strong prior dependence.

We conclude that with the experimental information provided by the assumed ATLAS measurement it will be challenging to perform a completely reliable parameter reconstruction and model comparison outside of the simplest CMSSM.

Acknowledgments

AJF is supported by the Science Technology and Facilities Council. LR is funded in part by the Foundation for Polish Science and by the EC 6th Framework Program MRTN-CT-2006-035505. We have used the `SuperBayeS` computer

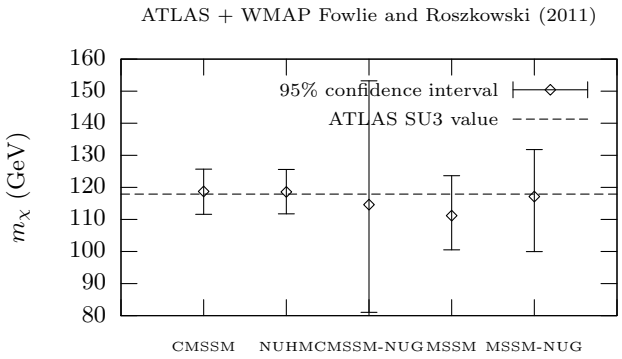

(a) m_χ reconstruction, with simulated LHC and simulated WMAP constraints

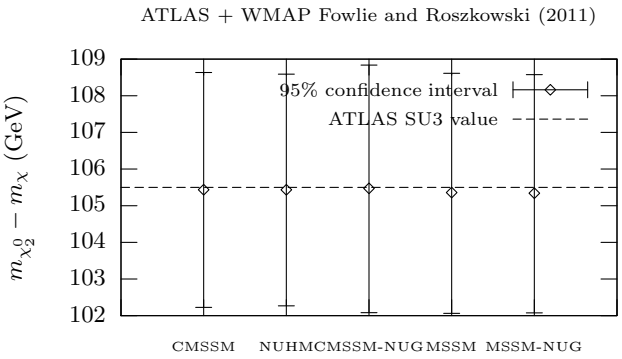

(b) $m_{\chi_2^0} - m_\chi$ reconstruction, with simulated LHC and simulated WMAP constraints

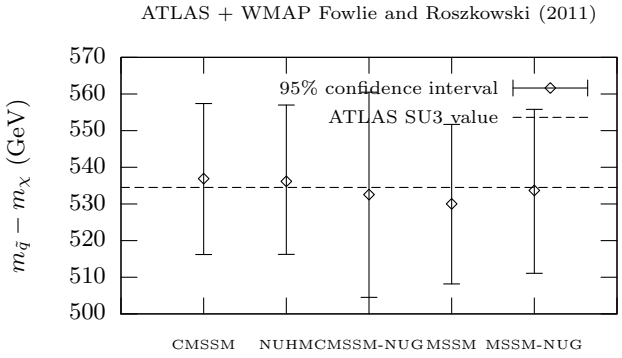

(c) $m_{\tilde{q}} - m_\chi$ reconstruction, with simulated LHC and simulated WMAP constraints

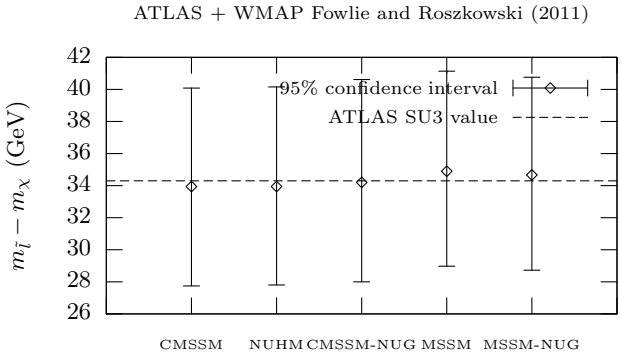

(d) $m_{\tilde{l}} - m_\chi$ reconstruction, with simulated LHC and simulated WMAP constraints

FIG. 17: The two-sigma (95%) confidence intervals and posterior means for m_χ (a), $m_{\chi_2^0} - m_\chi$ (b), $m_{\tilde{q}} - m_\chi$ (c) and $m_{\tilde{l}} - m_\chi$ (d).

program, which includes the independently developed codes `SOFTSUSY`, `micrOMEGAs` and `MultiNest` and some of the `CosmoMC` package routines. We thank Roberto Ruiz de Austri, who adapted `SuperBayeS` so that it scanned the MSSM-NUG and provided us with the adapted code. We also thank C. Topfel and M. Weber for providing the covariance matrix used in the ATLAS Collaboration Report (Ref. [6]).

[1] S. P. Martin (1997), hep-ph/9709356.
[2] D. Kazakov, Nucl.Phys. Proc. Suppl. **203-204**, 118 (2010), 1010.5419.
[3] I. Aitchison, Supersymmetry in Particle Physics. An Elementary Introduction (2007).
[4] P. Nath, B. D. Nelson, H. Davoudiasl, B. Dutta, D. Feldman, et al., Nucl. Phys. Proc. Suppl. **200-202**, 185 (2010), 1001.2693.
[5] A. Datta, G. L. Kane, and M. Toharia (2005), hep-ph/0510204.
[6] G. Aad et al. (ATLAS Collaboration) (2009), 0901.0512.
[7] R. Ruiz de Austri, R. Trotta, and L. Roszkowski, JHEP **05**, 002 (2006), hep-ph/0602028.
[8] R. Trotta, R. Ruiz de Austri, and L. Roszkowski, New Astron. Rev. **51**, 316 (2007), astro-ph/0609126.
[9] L. Roszkowski, R. Ruiz de Austri, and R. Trotta, JHEP **04**, 084 (2007), hep-ph/0611173.
[10] L. Roszkowski, R. Ruiz de Austri, R. Trotta, and J. Silk (2007), arXiv:0707.0622 [astro-ph].
[11] G. L. Kane, C. F. Kolda, L. Roszkowski, and J. D. Wells, Phys. Rev. **D49**, 6173 (1994), hep-ph/9312272.
[12] J. R. Ellis, K. A. Olive, and Y. Santoso, Phys. Lett. **B539**, 107 (2002), hep-ph/0204192.
[13] H. Baer, A. Mustafayev, E.-K. Park, and X. Tata, JHEP **0805**, 058 (2008), 0802.3384.

[14] L. Roszkowski, R. Ruiz de Austri, R. Trotta, Y.-L. S. Tsai, and T. A. Varley, Phys. Rev. **D83**, 015014 (2011), 0903.1279.
[15] L. Roszkowski, R. Ruiz de Austri, and R. Trotta, Phys. Rev. **D82**, 055003 (2010), 0907.0594.
[16] B. C. Allanach, Comput. Phys. Comm. **143**, 305 (2002), hep-ph/0104145.
[17] J. Dunkley et al. (WMAP Collaboration), Astrophys. J. Suppl. **180**, 306 (2009), 0803.0586.
[18] G. Belanger, F. Boudjema, A. Pukhov, and A. Semenov, Comput. Phys. Comm. **174**, 577 (2006), hep-ph/0405253.
[19] G. Belanger, F. Boudjema, A. Pukhov, and A. Semenov, Comput. Phys. Comm. **149**, 103 (2002), hep-ph/0112278.
[20] F. Feroz, M. P. Hobson, and M. Bridges (2008), 0809.3437.
[21] G. Belanger, S. Kraml, and A. Pukhov, Phys. Rev. **D72**, 015003 (2005), hep-ph/0502079.
[22] B. C. Allanach, S. Kraml, and W. Porod, JHEP **03**, 016 (2003), hep-ph/0302102.
[23] M. M. Nojiri et al. (2008), 0802.3672.
[24] J. Odier, Talk at the GDR Terascale meeting, Grenoble (2009).